

# Understanding the copper–phenoxyl radical array in galactose oxidase: contributions from synthetic modeling studies

Brian A. Jazdzewski, William B. Tolman \*

*Department of Chemistry, Center for Metals in Biocatalysis, University of Minnesota,  
207 Pleasant Street SE, Minneapolis, MN 55455, USA*

Received 24 November 1999; accepted 24 February 2000

## Contents

Abstract . . . . .	633
1. Introduction . . . . .	634
2. Biochemical and biophysical studies of GAO . . . . .	635
3. Structural and spectroscopic models of GAO . . . . .	640
3.1 Complexes containing bis(pyridyl)alkylamines . . . . .	640
3.2 Complexes containing mono(pyridyl)alkylamines . . . . .	646
3.3 Complexes containing triazacyclononanes . . . . .	648
3.4 Complexes containing salen and reduced salen ligands . . . . .	659
3.5 Complexes containing substituted hydrotris(pyrazoyl)borates . . . . .	663
3.6 Complexes containing other supporting ligands . . . . .	666
4. Complexes that model the reactivity of GAO . . . . .	672
5. Conclusions. . . . .	681
Acknowledgements . . . . .	682
References . . . . .	682

## Abstract

The two-electron oxidation of primary alcohols with dioxygen to yield aldehyde and hydrogen peroxide that is catalyzed by galactose oxidase (GAO) occurs at an intriguing active site comprising of a copper ion ligated by an unusual cysteine-modified tyrosine group. Both the metal ion and the tyrosinate undergo 1-electron redox interconversions during catalysis, the Cu(II)–tyrosyl radical form being a critical species. Due to the novelty of this

\* Corresponding author. Tel.: +1-612-6254061; fax: +1-612-6247029.

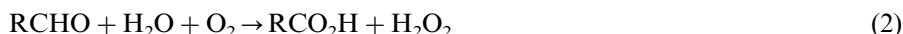
*E-mail address:* tolman@chem.umn.edu (W.B. Tolman).

coupled metal–radical cofactor unit in chemistry and biology and its importance within the more general context of radical–enzyme biochemistry, chemists have attempted to prepare model complexes for this and other redox-related states of GAO. The primary goals of such research are to better understand the enzyme active site spectral properties, structural attributes, and reactivity. In this review article, progress toward these goals is surveyed, beginning with a discussion of the synthesis and structural and spectroscopic characterization of model complexes of the GAO active site and ending with a description of more recent discoveries of catalytic reactivity by Cu(II)–phenoxyl radical species that replicate and provide insights into GAO function. © 2000 Elsevier Science S.A. All rights reserved.

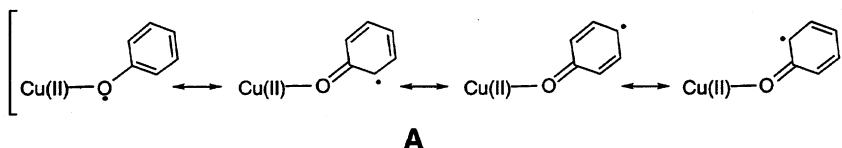
**Keywords:** Galactose oxidase; Phenoxyl radicals; Copper; Oxidation; Phenolate complexes

## 1. Introduction

Synergism between redox active metal centers and proximal organic cofactors is critically important for the catalysis of a wide range of multielectron reactions by enzymes [1,2]. A fascinating example is galactose oxidase, GAO, a small (68.5 kDa) monomeric, extracellular fungal enzyme which catalyzes the oxidation of primary alcohols to aldehydes, concomitant with the conversion of O<sub>2</sub> to H<sub>2</sub>O<sub>2</sub> (Eq. (1)) [3,4]. The H<sub>2</sub>O<sub>2</sub> produced is apparently used for lignin degradation by peroxidases excreted by the fungus. A related enzyme (with a similar active site) is glyoxal oxidase, GLO [5,6], which also generates H<sub>2</sub>O<sub>2</sub> but does so according to Eq. (2).



Detailed structural, spectroscopic, and kinetic studies have shown that the 2-electron reaction catalyzed by GAO is performed within an active site that contains a single copper ion that shuttles via 1-electron processes between the +I and +II oxidation states [1,3,4]. This apparent paradox (2-electron chemistry by a single Cu ion) is resolved by the involvement of another redox active cofactor in catalysis, identified as a copper-coordinated tyrosinate that is oxidized to a tyrosyl radical during the catalytic cycle. In particular, spectroscopic data have been interpreted to indicate that a key reactive species contains a magnetically coupled Cu(II)–tyrosyl radical unit (**A**), which is responsible for the oxidation of primary alcohol substrates. Thus, by juxtaposing two units that readily undergo single electron redox reactions [Cu(I)/Cu(II) and tyrosinate/tyrosyl radical], an overall 2-electron process is catalyzed.



Until recently, metal–phenoxyl radical units such as **A** were unknown in coordination chemistry. Stimulated by its novelty, its postulated involvement in catalysis by GAO, and the growing realization of the general importance of metal–radical cofactor arrays in enzymatic catalysis, chemists have attempted to synthesize and characterize complexes that contain a metal–phenoxyl radical unit as models for **A**. In addition, significant efforts have been made to construct models of other postulated intermediates in the GAO catalytic cycle. Together, these studies have provided important insights into the structure, physiochemical properties, and function of the enzyme. In addition, the knowledge obtained has led to the recent development of synthetic catalysts that mimic both the structure and function of GAO, a true ‘bioinorganic success story’ [7]. In this review we survey this progress in synthetic modeling of the active site chemistry of GAO. A brief overview of the biochemical and biophysical studies of the enzyme is a necessary preamble for defining the key issues addressed by the synthetic work. Next, we present research results from various synthetic studies that have contributed to our understanding of the structural, spectroscopic, and magnetic properties of GAO active site intermediates. The discussion of these studies is organized by the chelating ligand type because of the structural similarities of the complexes supported by each ligand class. We then describe reactivity studies, mechanistic implications, and biomimetic catalyst development of relevance to the enzyme.

## 2. Biochemical and biophysical studies of GAO

The salient aspects of the structure and properties of GAO have been reviewed [1–4,8,9], so only a brief description will be provided here. A view of the active site drawn from X-ray crystallographic data (Fig. 1; pH 4.5, 1.7 Å resolution) reveals

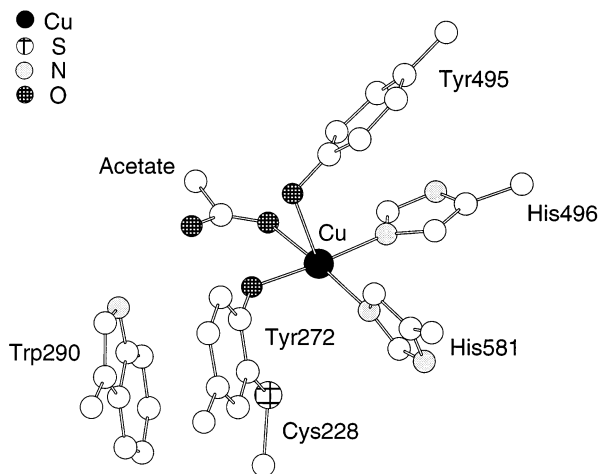


Fig. 1. Drawing of the active site of GAO, as determined by X-ray crystallography (pH 4.5) [10].

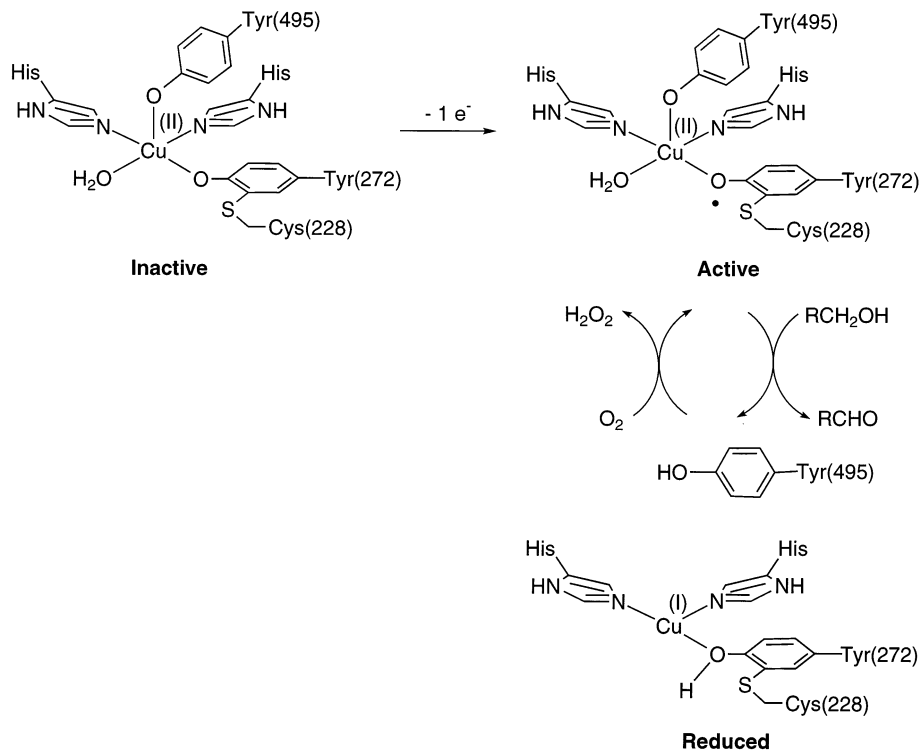


Fig. 2. Schematic representation of the active site of GAO in its three redox forms.

a single copper ion in a square pyramidal geometry [10]. Two histidine imidazolyls, a tyrosine phenolate (Y272), and an acetate ion from the crystallization buffer are coordinated in the equatorial plane, while Y495 resides in the axial position with a long Cu–O distance (2.7 Å). At pH 7.0 in Pipes buffer, the acetate is replaced by a water molecule ~2.8 Å from the Cu ion, resulting in a metal geometry better described as distorted tetrahedral. Although it is clear that Y272 is a deprotonated phenolate ligand, spectral evidence (vide infra) suggests that Y495 may be protonated in the form of the enzyme characterized by crystallography. Importantly, the X-ray structural data revealed that Y272 is covalently linked to a cysteine (C228) via a bond between the cysteine and the tyrosine C<sub>6</sub>. This unusual thioether-modified Y272  $\pi$ -stacks with the indole ring of a tryptophan residue (W290; 3.4 Å interplanar distance).

Three redox states of the enzyme have been identified by spectroscopic studies [3,4]. When isolated, GAO exists as a mixture of Inactive and Active forms which Whittaker showed may be isolated independently by treatment with 1-electron redox agents (Fig. 2). The Inactive form resulting from treatment of the native enzyme with K<sub>4</sub>Fe(CN)<sub>6</sub> contains Cu(II) with phenolate ligation as shown by EPR, X-ray absorption (XANES, EXAFS), UV–vis, and resonance Raman spectroscopy

(Table 1). Notably, this assignment is supported by the presence of an axial signal in the EPR spectrum with Cu-hyperfine features [9,11–13]. As implied by its name, this form is incapable of performing the enzymatic reaction, and its spectroscopic features are unperturbed by incubation with the substrate or O<sub>2</sub>.

Treatment of the Inactive form with 1-electron oxidants generates the Active form, which is capable of oxidizing the substrate. XANES experiments showed that the Active form also contains Cu(II) [14] and EXAFS data demonstrated that there was no significant structural change at the active site upon oxidation [13]. This form also contains an organic radical cofactor, as indicated by the absence of an EPR signal and the presence of unusual UV–vis features (Table 1). The cofactor was suggested to be the cysteine-modified Y272 on the basis of EPR and ENDOR analysis of the free radical generated upon oxidation of the metal-free enzyme (apo-GAO) [15]. In addition, resonance Raman spectra for the Active form contained features diagnostic for a phenoxyl radical and a phenolate, with the latter disappearing upon addition of azide [16]. The azide addition was accompanied by the generation of a N<sub>3</sub><sup>−</sup> → Cu(II) charge transfer (CT) band in the absorption spectrum and the uptake of a proton at the active site by a residue with pK<sub>a</sub> > 9. On the basis of these observations, it was suggested that (i) azide was bound to the equatorial site (where acetate or water was identified in the X-ray structure); and

Table 1  
Summary of selected properties of various forms of GAO

Compound	UV–vis $\lambda_{\text{max}}$ , nm ( $\epsilon$ , M <sup>−1</sup> cm <sup>−1</sup> )	EPR <sup>a</sup>	Resonance Raman shifts (cm <sup>−1</sup> )
Active GAO	444(5194), 800(3211) <sup>b</sup>	EPR silent	1170, 1185, 1246, 1310, 1382, 1416, 1439, 1479, 1487, 1595, 1603 <sup>c</sup>
Inactive GAO	438(1000), 625(1167) <sup>b</sup>	$g_{\parallel} = 2.277$ , $g_{\perp} = 2.055$ , $A_{\parallel} = 186$ <sup>d</sup>	<sup>e</sup>
Reduced GAO <sup>f</sup>	$\approx 450(\leq 500)$ , $\approx 650(\leq 500)$ <sup>g</sup>	EPR silent	<sup>e</sup>
Active GAO + N <sub>3</sub> <sup>−</sup> <sup>h</sup>	383(4218), 499(3654), 890 (1218) <sup>b</sup>	EPR silent	1185, 1246, 1312, 1417, 1439, 1490, 1595 <sup>i</sup>
Apo-GAO	$\approx 450, 800$ <sup>j</sup>	$g_{\text{av}} = 2.0055$ <sup>k</sup>	<sup>e</sup>

<sup>a</sup> X-band EPR data, with  $A$  values reported in units of 10<sup>−4</sup> cm<sup>−1</sup>.

<sup>b</sup> Ref. [5].

<sup>c</sup>  $\lambda_{\text{ex}} = 875$  nm. Ref. [16].

<sup>d</sup> (a) R.D. Bereman, D.J. Kosman, J. Am. Chem. Soc. 99 (1977) 7322. (b) Ref. [11].

<sup>e</sup> Data not reported.

<sup>f</sup> Prepared upon reaction of active GAO with 1-*O*-methyl- $\beta$ -D-galactopyranoside under Ar; Ref. [11].

<sup>g</sup> Ref. [11].

<sup>h</sup> Prepared by reaction of active GAO with excess N<sub>3</sub><sup>−</sup>; Ref. [16].

<sup>i</sup>  $\lambda_{\text{ex}} = 647.1$  nm; Ref. [16].

<sup>j</sup> More exact values for  $\lambda_{\text{max}}$  and  $\epsilon$  not reported.

<sup>k</sup> Refs. [15,18].

(ii) protonation and decomplexation of Y495 occurred leaving the Y272 radical unperturbed [11,12,17]. To explain the lack of an EPR signal in the Active form, antiferromagnetic coupling between Y272 $\cdot$  and the Cu(II) ion was invoked, with a splitting energy of 200 cm $^{-1}$  ( $S_T=0$  ground state) estimated from magnetic susceptibility measurements [9]. The feature in the UV–vis spectrum at 445 nm was attributed to a  $\pi \rightarrow \pi^*$  transition typical for phenoxyl radicals, while the intense 810 nm band was assigned as a combination of an unusual interligand CT involving Y272 $\cdot$  and Y495 along with Cu(II) ligand field features [16]. This assignment is supported by the finding that when the axial tyrosine is mutated to a phenylalanine (Y495F) the active site may be oxidized, but the 810 nm absorption is absent in the resulting UV–vis spectrum [17]. The Cu(II)–Y272 $\cdot$  array as well as Y272 $\cdot$  in apo-GAO are quite stable despite their accessibility to solvent. Interestingly, the oxidation potential of the modified Y272 in apo-GAO ( $\sim + 0.4$  V [18]) is significantly lower than free tyrosine (0.93 V [19]) or other redox active tyrosine residues in proteins (e.g. 1.0 V in ribonucleotide reductase [20]), signifying enhanced stability of the radical due to the thioether substituent, the stacking tryptophan residue, and/or other factors.

Addition of substrate under anaerobic conditions to the stable active enzyme or incubation with sodium dithionite generates the third isolable form, Reduced (Fig. 2). This form contains Cu(I) as indicated by XANES [14] and lacks a signal in its EPR spectrum (Table 1). The results of an EXAFS study [21] were interpreted to indicate coordination of three N,O ligands bound to Cu at an average distance of 1.99 Å. It was presumed that both Y272 and Y495 are protonated and that both histidine ligands are bound to Cu(I) in this form, but further structural information is scant. Importantly, and consistent with its overall formulation, addition of O $_2$  to the Reduced form yields the Active form and, presumably, H $_2$ O $_2$  (although it appears not to have been identified unequivocally for such a single turnover reaction).

Using the structures proposed for the various forms of the enzyme as a starting point with additional information from kinetic [22], radical probe [23,24], and computational modeling studies [25], a ping-pong mechanism for GAO has been put forth (Fig. 3). In the first phase (substrate oxidation), galactose is proposed to coordinate to the Cu(II) in an equatorial position of the Active form (occupied by water or acetate in the X-ray structures of the native enzyme). The Y495 then deprotonates the alcohol followed by H-atom abstraction by the O-atom of the coordinated Y272 $\cdot$  radical. A large H/D kinetic isotope effect (KIE) of 22 at 4°C for this step confirmed that it is rate-controlling in the catalytic cycle, with a tunneling contribution to the H-atom transfer implicated by a large temperature dependence [22]. The H-atom abstraction is stereospecific, as shown by the removal of the *pro-S* hydrogen from deuterium labeled  $\beta$ -D-galactopyranoside substrate [26]. The oxidative phase is completed by intramolecular electron transfer from the putative ketyl radical to Cu(II) followed by the loss of aldehyde, generating the Reduced form of the enzyme. Whether the overall process involves H-atom abstraction followed by electron transfer, the reverse (electron transfer to Cu(II) followed by H-atom abstraction), or a concerted atom/electron transfer process is

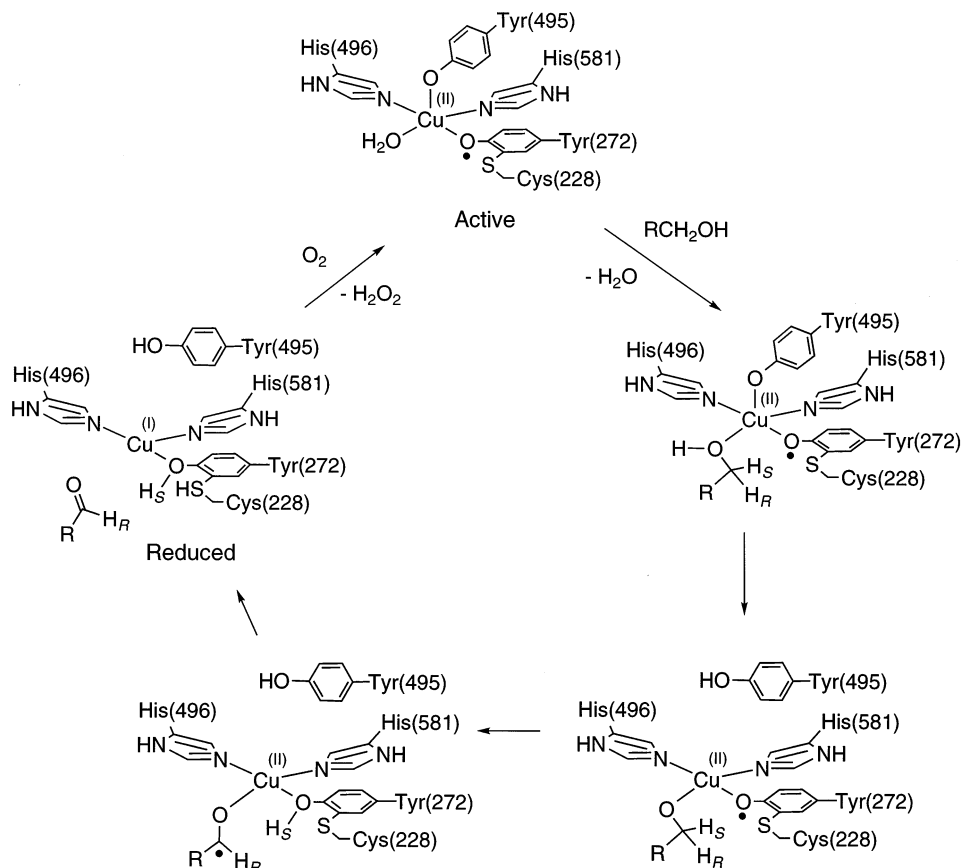


Fig. 3. Proposed mechanism for D-galactose oxidation by GAO (R = pyranose ring associated with D-galactose) [3,4].

difficult to distinguish unambiguously from the available data, but the overall nature of the reaction involving rate-determining substrate C–H bond breaking by the Cu-coordinated Y272 $\cdot$  radical is clear. The second phase of the mechanism involves oxidation of the Reduced form to the Active form by  $\text{O}_2$ , which is converted to  $\text{H}_2\text{O}_2$  using the protons available from substrate. Presumably, a Cu(II)–hydroperoxide is involved as an intermediate in this process, although no such species has been observed during this fast phase.

As the aforementioned understanding of GAO has developed through biochemical and biophysical studies, issues of great interest have arisen which have stimulated efforts by synthetic chemists to construct compounds that model aspects of the active site structures and properties of the various forms of the enzyme. Questions raised include: What is the role of the cysteine–tyrosinate covalent modification? How may spectroscopic properties of the various redox forms of the enzymes be rationalized? Is it possible to construct a Cu(II)–tyrosyl radical array

within a model complex? If so, how might the stability, spectral properties, and reactivity of such a synthetic array compare to that found in GAO? Can mononuclear Cu(I)–phenol(ate) complexes that model the Reduced form of GAO be prepared, and will they react analogously to the enzyme? Finally, can the reactivity of GAO be mimicked in a synthetic system, and if so, what mechanistic conclusions of relevance to the enzyme can be drawn? While definitive answers to all aspects of the issues raised by these questions are not yet available, considerable progress has been made in replicating structural and spectroscopic features of the key redox forms, probing the role of the cysteine–tyrosinate linkage, rationalizing spectroscopic and magnetic features, providing mechanistic information on enzyme function, and using this knowledge to develop novel abiological catalysts.

### 3. Structural and spectroscopic models of GAO

In general, while mononuclear Cu(II)–phenolate complexes are common, Cu(II)–phenoxyl radical and Cu(I)–phenol(ate) complexes are quite rare. A common synthetic strategy used to construct such complexes as models for the Inactive, Active and Reduced forms of GAO, respectively, has been to use multidentate ligands comprising multiple N-donors linked to one or more phenol arms. This approach is taken in order to disfavor decomplexation of the coordinated phenolate or phenoxyl radicals during redox reactions, thus allowing closer replication of enzyme spectroscopic properties and reactivity. Such ligands based on the mono- and bis(pyridyl)alkylamine, 1,4,7-triazacyclononane (TACN), and *N,N'*-alkyl-bis(-salicylimine) (salen) frames have been most thoroughly studied, since they are well-known to be of general utility in transition metal chemistry and to be particularly useful for the isolation and characterization of copper complexes. A few studies have also focused on reacting exogenous phenolates with Cu(II) centers supported by N-donor ligands such as functionalized hydrotris(pyrazoyl)borates and polyamines. In the following subsections that are organized according to supporting ligand type, we survey complexes designed to model one or more of the three forms of GAO (summarized schematically in Fig. 2). The relationships between the structural and spectroscopic features of the complexes to those exhibited by the enzyme will be emphasized. Aspects of the reactivity of some of these compounds will be presented in Section 4.

#### 3.1. Complexes containing bis(pyridyl)alkylamines

Several research groups have used ligands that have in common, bis(pyridyl)alkylamines linked to a single phenol (Fig. 4) [27]. This basic tripodal ligand design has been varied by adjusting the length of the alkyl chain linking the pyridine and tertiary amine donors (*x* and *y*), as well as by changing the phenol ring substituents ( $R_1$  and  $R_2$ ). Numerous mononuclear complexes of the general formula LCuX (X = monoanionic donor ligand, such as  $Cl^-$  or  $CH_3CO_2^-$ , L = phenolate-containing bis(pyridyl)alkylamine ligand) have been prepared (Table 2). Two

Table 2

Summary of selected properties of monomeric Cu(II) complexes of  $L^-$  (HL = bis(pyridyl)alkylamine ligand shown in Fig. 4, with  $R_1 = H$ )

No.	Formula	$x$	$y$	$R_2$	UV-vis $\lambda_{\max}$ , nm ( $\epsilon$ , $M^{-1} \text{ cm}^{-1}$ ) <sup>a</sup>	EPR <sup>b</sup>	Ref.
1	LCuCl·2H <sub>2</sub> O	2	2	H	260 (11200), 290 (sh, 5220), 440 (1940), 670 (220)	$g_{\parallel} = 2.25$ , $g_{\perp} = 2.04$ , $A_{\parallel} = 147.0$	[28]
2	LCuN <sub>3</sub> ·H <sub>2</sub> O	2	2	H	240 (11400), 280 (sh, 5280), 405 (2310), 465 (sh, 1380), 650 (260)	$g_{\parallel} = 2.23$ , $g_{\perp} = 2.04$ , $A_{\parallel} = 156$	[28]
3	LCuCl	1	1	NO <sub>2</sub>	248 (24100), 375 (27860), 690 (260)	$g_{\parallel} = 2.217$ , $g_{\perp} = 2.098$ , $A_{\parallel} = 173$ , $A_{\perp} = 31$	[29,30]
4	LCu(SCN)	1	1	NO <sub>2</sub>	251 (17200), 383 (26100), 667 (225)	$g_{\parallel} = 2.227$ , $g_{\perp} = 2.052$ , $A_{\parallel} = 187$ , $A_{\perp} = 36$	[30]
5	LCuN <sub>3</sub> ·H <sub>2</sub> O	1	1	NO <sub>2</sub>	248 (9300), 317 (26100), 386 (16590), 662 (280), 1000 (75)	$g_{\parallel} = 2.327$ , $g_{\perp} = 2.081$ , $A_{\parallel} = 187$ , $A_{\perp} = 4$	[30]
6	LCu(O <sub>2</sub> CCMe <sub>3</sub> )·H <sub>2</sub> O	1	2	H	253 (12900), 300 (sh, 4300), 460 (400), 670 (110)	<sup>c</sup>	[31]
7	LCuCl·H <sub>2</sub> O	1	2	NO <sub>2</sub>	257 (17100), 400 (30000), 680 (210)	<sup>c</sup>	[31]
8	LCu(O <sub>2</sub> CCMe <sub>3</sub> )·H <sub>2</sub> O	1	2	NO <sub>2</sub>	257 (12000), 404 (23500), 645 (140)	<sup>c</sup>	[31]
9	LCuCl·2H <sub>2</sub> O	2	2	NO <sub>2</sub>	257 (7800), 378 (15300), 760 (160)	<sup>c</sup>	[31]
10	LCu(O <sub>2</sub> CMe)·H <sub>2</sub> O	2	2	NO <sub>2</sub>	260 (11000), 395 (19000), 675 (320)	<sup>c</sup>	[31]
11	LCu(SCN)·MeCO <sub>2</sub> Et	2	2	NO <sub>2</sub>	260 (12082), 386 (18885), 665 (225)	<sup>c</sup>	[31]
12	LCu(O <sub>2</sub> CMe)	1	2	NO <sub>2</sub>	256 (14200), 405 (18600), 669 (210)	<sup>c</sup>	[32]
13	LCu(O <sub>2</sub> CC <sub>6</sub> H <sub>4</sub> p-NO <sub>2</sub> )	1	1	H	264 (22100), 669 (90)	<sup>c</sup>	[32]
14	LCu(O <sub>2</sub> CMe)·H <sub>2</sub> O	1	1	NO <sub>2</sub>	256 (11200), 401 (17650), 685 (140)	<sup>c</sup>	[32]
15	LCu(O <sub>2</sub> CPh)	1	1	NO <sub>2</sub>	257 (12600), 438 (600), 780 (140)	<sup>c</sup>	[32]

<sup>a</sup> All spectra in CH<sub>3</sub>CN solvent, except complexes **3–5** (MeOH) and complex **9** (1:1 DMF/CH<sub>3</sub>CN).<sup>b</sup> Data obtained at X-band frequency, with  $A$  values in units of  $10^{-4} \text{ cm}^{-1}$ . For complexes **1** and **2** the solvent was 1:1 DMF/CH<sub>3</sub>Cl; for complexes **3–5**, the solvent was MeOH.<sup>c</sup> EPR data not reported.

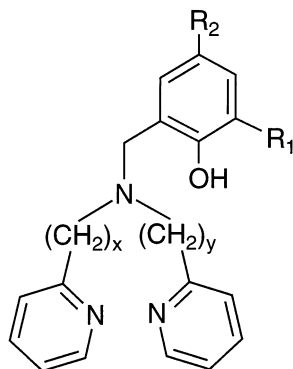


Fig. 4. General representation of the bis(pyridyl)alkylamine ligand framework, HL ( $x = y = 1$  or  $2$ ,  $R_1 = R_2 =$  alkyl substituents).

additional compounds,  $[\text{HLCuCl}]\text{ClO}_4 \cdot \text{MeOH}$  (**16**,  $x = y = 1$ ,  $R_2 = \text{H}$ ) and  $[\text{HLCuCl}]\text{PF}_6 \cdot \text{MeOH}$  (**17**,  $x = y = 1$ ,  $R_2 = \text{Br}$ ), have been structurally characterized (vide infra), but are not included in Table 2 because no spectral data were reported. Characteristic features of compounds **1–15** include a phenolate  $\rightarrow \text{Cu(II)}$  CT transition in their UV–vis spectra ( $\lambda_{\text{max}} \approx 380\text{--}450$  nm) as well as axial signals in their EPR spectra. Many of these complexes also have been characterized by X-ray crystallography (cf. Fig. 5) [28–33]. All of the structures confirm that the supporting ligand provides two pyridyl, one tertiary amine, and one phenolate donor, with the copper coordination sphere completed by  $\text{X}^-$ . The phenolate donor can bind either in an equatorial or axial position in what are typically square pyramidal complexes. Comparisons of systems that differ with respect to the phenolate

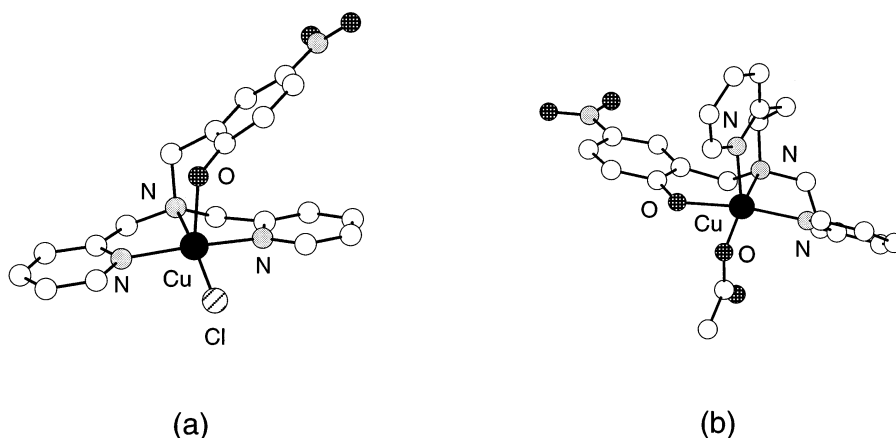


Fig. 5. X-ray crystal structures of (a) **3**, which contains two five-membered chelate rings and the phenolate in the axial position [29,30] and (b) **10**, which contains three six-membered chelate rings and the phenolate in an equatorial position [31].

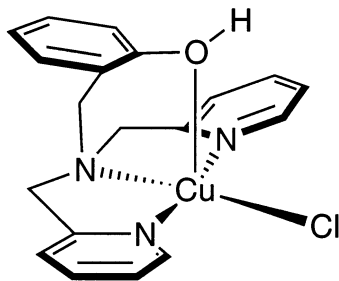


Fig. 6. Schematic representation of the structure of the Cu(II)–phenol complex **16** [33].

substituents or the alkyl linker arm lengths indicate that it is the latter that governs phenolate disposition [31,32]. Thus, axial coordination can be induced if short spacers resulting in five-membered chelate rings are present (Fig. 5a), while equatorial binding is favored for ligands with only ethyl linkers, thus forming six-membered chelates (Fig. 5b). Attainment of axial phenolate coordination has been emphasized as an important objective for modeling the long (2.7 Å) Y495–Cu interaction in GAO, but only when the axial phenolate is protonated has the approximate replication of the protein structural data been achieved (**16**, Fig. 6; Cu–O = 2.565 Å) [33]. These data are consistent with the hypotheses that Y495 is protonated in the protein crystal structures and that it may act as a base during catalysis.

When the syntheses using bis(pyridyl)alkylamine/phenol ligands were performed in the absence of a strong monoanionic donor (e.g. with  $\text{Cu}(\text{ClO}_4)_2$ ,  $\text{Cu}(\text{CF}_3\text{SO}_3)_2$ ,  $\text{Cu}(\text{BF}_4)_2$ , or  $\text{CuSO}_4$ ), dimeric complexes of the formulation  $[\text{LCu}]_2^{2+}$  were isolated (**18–31**, Table 3) [31,32,34–37]. A representative X-ray structure of one of them (**19**) is shown in Fig. 7. All structurally characterized complexes similar to **19** show two Cu(II) ions in square pyramidal geometries, with slight trigonal bipyramidal distortions. The metal ions are bridged by two phenolates, one from each ligand. As seen in their mononuclear analogs, the phenolate ligand can reside in either an axial or equatorial position depending on steric constraints imposed by chelate ring size. Like the monomeric complexes discussed above, the UV–vis spectra of the dimeric complexes exhibit a phenolate  $\rightarrow$  Cu(II) CT band as well as d–d transitions at a lower energy in their UV–vis spectra. EPR data are generally not reported [38], presumably due to strong antiferromagnetic coupling of the phenolate-bridged Cu(II) ions that results in diamagnetic ground states for the compounds.

The isolation of dicopper complexes **18–31** is unfortunate, since such dimers are not desired for accurate mimicry of the monocopper GAO active site. Attempts to dissociate these dimers by addition of an exogenous ligand (e.g. phenol, *p*-cresol or imidazole in the presence of NaOH) proved to be unsuccessful in most cases [31]. However, addition of excess pyridine to complexes **29** and **30** was reported to yield monomers similar to those listed in Table 2 [36]. These monomers were characterized by UV–vis and EPR spectroscopy and cyclic voltammetry. Evidence for monomer formation upon addition of pyridine includes a 20–50 nm red shift of

Table 3

Summary of UV–vis data of dimeric Cu(II) complexes of L<sup>−</sup> (HL = bis(pyridyl)alkylamine ligand shown in Fig. 4)

No.	Formula	x	y	R <sub>1</sub>	R <sub>2</sub>	UV–vis $\lambda_{\max}$ , nm ( $\epsilon$ , M <sup>−1</sup> cm <sup>−1</sup> ) <sup>a</sup>	Ref.
18	[LCu] <sub>2</sub> (BF <sub>4</sub> ) <sub>2</sub>	2	2	H	H	440(5730) <sup>b</sup>	[34]
19	[LCu] <sub>2</sub> (ClO <sub>4</sub> ) <sub>2</sub> ·H <sub>2</sub> O	2	2	H	H	263(13000), 439(4000), 660(365)	[35]
20	[LCu] <sub>2</sub> (ClO <sub>4</sub> ) <sub>2</sub> ·H <sub>2</sub> O	1	2	H	H	257(12600), 287(sh, 6400), 438(600), 780(140)	[31]
21	[LCu] <sub>2</sub> (CF <sub>3</sub> SO <sub>3</sub> ) <sub>2</sub>	2	2	H	H	262(10200), 439(3150), 660(350)	[31]
22	[LCu] <sub>2</sub> (ClO <sub>4</sub> ) <sub>2</sub> ·2H <sub>2</sub> O	1	2	H	NO <sub>2</sub>	257(13200), 401(25800), 655(175)	[31]
23	[LCu] <sub>2</sub> (BF <sub>4</sub> ) <sub>2</sub> ·2H <sub>2</sub> O	1	2	H	NO <sub>2</sub>	256(15500), 400(28200), 640(165)	[31]
24	[LCu] <sub>2</sub> (ClO <sub>4</sub> ) <sub>2</sub> ·2H <sub>2</sub> O	2	2	H	NO <sub>2</sub>	258(13200), 374(19000), 680(150)	[31]
25	[LCu] <sub>2</sub> (BF <sub>4</sub> ) <sub>2</sub> ·2H <sub>2</sub> O	2	2	H	NO <sub>2</sub>	258(13200), 374(19000), 680(150)	[31]
26	[LCu] <sub>2</sub> (ClO <sub>4</sub> ) <sub>2</sub> ·H <sub>2</sub> O	1	1	H	H	257(11200), 291(sh, 6150), 839(190)	[32]
27	[LCu] <sub>2</sub> (BF <sub>4</sub> ) <sub>2</sub>	1	1	H	H	257(12000), 290(sh, 6500), 840(200)	[32]
28	[LCu] <sub>2</sub> (SO <sub>4</sub> )	1	1	H	NO <sub>2</sub>	252(8250), 257(11750), 391(10850), 402(20600), 690(130), 794(120)	[32]
29	[LCu] <sub>2</sub> (PF <sub>6</sub> ) <sub>2</sub>	2	2	SMe	Me	520(2800), 700(675) <sup>b</sup>	[36]
30	[LCu] <sub>2</sub> (PF <sub>6</sub> ) <sub>2</sub>	2	2	H	Me	455(3340), 665(413) <sup>b</sup>	[36]
31	[LCu] <sub>2</sub> (PF <sub>6</sub> ) <sub>2</sub>	2	2	SMe	<i>t</i> -Bu	<sup>c</sup>	[37]

<sup>a</sup> All spectra in CH<sub>3</sub>CN solvent except complex **28** (H<sub>2</sub>O).<sup>b</sup> Full UV–vis data not reported.<sup>c</sup> No UV–vis data reported.

both the phenolate  $\rightarrow$  Cu(II) CT and d–d transitions, as well as a decrease in the intensity of these absorptions. Also, monomer formation was inferred on the basis of the appearance of an axial signal in the EPR spectra. Specific differences between the properties of **29**, **30**, and their derived monomeric species correlate with the presence or absence, respectively, of the thioether substituent on the phenolate portion of their supporting ligand(s). Thus, the UV–vis absorptions associated with both **29** and its monomeric pyridine adduct (with the thioether group) occur at lower energy than in the complexes that lack the thioether moiety (**30** and its pyridine adduct). Also, while both monomers exhibited reversible Cu(II)/Cu(I) couples at similar potentials, irreversible ligand based oxidative processes were observed and their potentials varied significantly; the monomer derived from **29** had an  $E_{p,a}$  (0.705 V vs. SCE) that was 200 mV lower than that of the monomer derived from **30**. This shift in potential of a coordinated phenolate due to the presence of a thioether substituent implicates a possible redox-tuning role for the cysteine modification in GAO. However, in other synthetic systems the potential shifts that result upon attachment of a thioether substituent to a coordinated phenolate are much smaller (vide infra). Thus, while thioether substituents would be expected to perturb the electrochemical properties of a coordinated phenolate through inductive effects, the contribution of such an effect in setting the GAO redox potential remains unclear.

In a very recent report [LCu]<sub>2</sub> dimer dissociation was observed upon addition of a chemical oxidant [37]. Treatment of **31** with Ce(NO<sub>3</sub>)<sub>6</sub>(NH<sub>4</sub>)<sub>2</sub> is believed to form the mononuclear Cu(II)–phenoxyl radical species, [31(NO<sub>3</sub>)]<sup>•+</sup>. While this does not represent the first example of such a complex in copper coordination chemistry

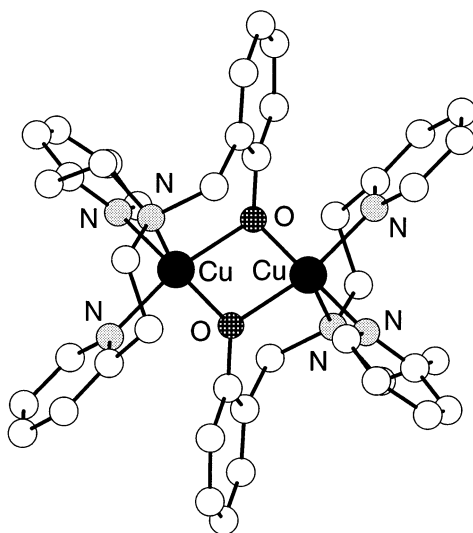


Fig. 7. X-ray crystal structure of the bis(phenolate)-bridged dimer **19** [35].

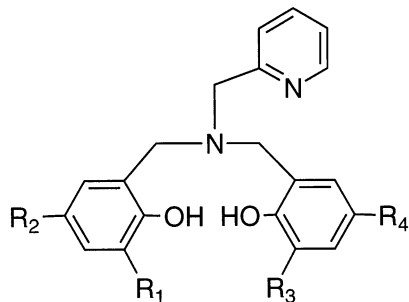


Fig. 8. General representation of the mono(pyridyl)alkylamine ligand framework ( $R_1 = R_2 = R_3 = R_4 =$  alkyl substituents).

(vide infra), this molecule does serve, as a unique instance of a Cu(II)–phenoxyl radical complex supported by a bis(pyridyl)alkyl amine ligand framework. While a more complete description of the properties of such complexes will be presented below, we note here that  $[31(\text{NO}_3)]^{*+}$  is similar to other such species, insofar as it is characterized by UV–vis absorptions at 418 and 887 nm, a lack of an EPR signal, and features in its resonance Raman spectroscopy consistent with a phenoxyl radical. This complex was found to be moderately stable at ambient temperatures ( $k_{\text{dec}} = 1.62 \times 10^{-3} \text{ s}^{-1}$ ) and capable of functioning as an alcohol oxidation catalyst (vide infra).

### 3.2. Complexes containing mono(pyridyl)alkylamines

Another class of GAO model complexes was built by using supporting ligands with two phenol groups attached to a mono(pyridyl)alkylamine frame (Fig. 8). The derived bis(phenolate) ligands were targeted in order to model the bis(tyrosinate) ligation of the GAO active site. Dimers analogous to those seen with bis(pyridyl)(phenol)alkylamines were observed in the solid state [39–41]. A representative crystal structure of one of these dimers can be seen in Fig. 9 (**32**,  $R_1 = \text{SMe}$ ,  $R_2 = R_3 = R_4 = \text{Me}$ ). Similar structures for complexes containing ligands with alternative phenolate substitution patterns have been reported (**33**,  $R_1 = R_2 = R_3 = R_4 = \text{H}$ ; **34**,  $R_1 = R_3 = R_4 = \text{H}$ ,  $R_2 = \text{SMe}$ ; **35**,  $R_1 = R_3 = t\text{-butyl}$ ,  $R_2 = R_4 = \text{H}$ ). Note that the two phenolate donors within each ligand in **32** and **34** differ; in this regard, these complexes model the mixed Y272-C228/Y495 tyrosinate ligation in GAO. In all of the structures, dicopper(II) cores are bridged by two phenolate groups, one from each ligand.

Dissociation of dimers **32**–**35** by either addition of exogenous donor ligands (e.g. pyridine, alcohols) or proton sources has been investigated. For example, addition of pyridine or  $\text{CH}_3\text{CN}$  to either **32** or **35** resulted in a shift of both the phenolate  $\rightarrow$  Cu(II) CT and d–d transitions to lower energy (50–75 nm), a decrease in intensity of these absorption features, and the appearance of an axial signal in EPR spectra

[39,40]. As noted above, such evidence indicates monomer formation. The electrochemical properties of these monomers were investigated, revealing two quasi-reversible or irreversible oxidations at high potential (0.4–0.9 V vs. SCE) [42] corresponding to successive ligand oxidations. Controlled potential electrolysis of the monomer derived from **35** in CH<sub>3</sub>CN led to the formation of a fairly stable intermediate ( $t_{1/2} \sim 9$  h) that was suggested to be a Cu(II)–phenoxyl radical species which models Active GAO [41]. This species could also be generated chemically by reacting **35** in CH<sub>3</sub>CN with excess AgOAc. Its absorption spectrum was reported to contain features with  $\lambda_{\text{max}}$  at 439 ( $\epsilon$  16 700 M<sup>−1</sup> cm<sup>−1</sup>) and 620 (600 M<sup>−1</sup> cm<sup>−1</sup>) nm, roughly similar to those exhibited by Active GAO. Resonance Raman evidence was cited to support assignment of the species as a Cu(II)–phenoxyl radical. Surprisingly, this species was found to be EPR active, with a broad signal centered about  $g = 2$ . Other Cu(II)–phenoxyl radical compounds with different supporting ligands (vide infra), as well as Active GAO, had been shown to be EPR silent due to antiferromagnetic coupling of the radical and Cu(II) spins. The authors rationalized the observation of an EPR signal by invoking axial ligation of the phenoxyl radical, which somehow results in weak ferromagnetic coupling or a dipole–dipole interaction. Analysis of the organic products after decomposition of the species showed that ligand coupling occurred at the *para* position of one phenol ring from each ligand, indirectly supporting the hypothesis that a phenoxyl radical species was involved.

In a separate study, it was shown that **33** and **34** could be dissociated upon the addition of an acid, presumably to yield monomers with one protonated phenolate group that is suggested to remain coordinated to Cu(II) (Fig. 10) [40,41,43]. The process is fully reversible, with regeneration of the dimeric species upon addition of Et<sub>3</sub>N [44]. Monomer formation was inferred from the presence of an axial signal in

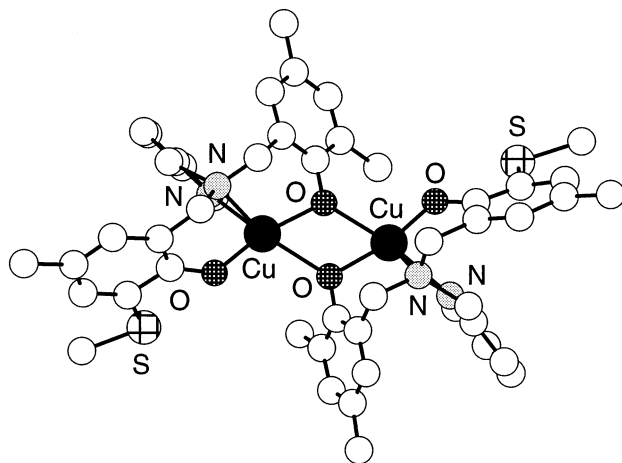


Fig. 9. X-ray crystal structure of the bis(phenolate)-bridged dimer **32** [39].

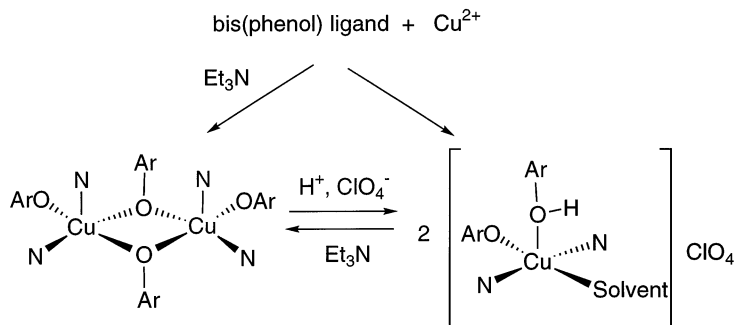


Fig. 10. Acid–base interconversions implicated in the studies of the Cu(II)–phenolate complexes **33** and **34** (Ar = aryl unit) [40].

the EPR spectra as well as  $\nu_{\text{OH}}$  stretches in IR spectra. These Cu(II)–(phenol)(phenolate) complexes serve as models for the mixed (tyrosine)(tyrosinate) ligation in GAO, but attempts to isolate these monomeric species only led to the recovery of dimers.

### 3.3. Complexes containing triazacyclononanes

The TACN framework provides a facially capping ligand and three secondary amine groups that may be readily derivatized to allow the incorporation of phenol and/or alkyl substituents (Fig. 11) [45]. Ligands bearing one, two, or three phenol groups have been synthesized with various *ortho* and *para* substituents. Examples of common phenol substituents include *t*-butyl, SMe, and OMe which serve to add steric bulk and help to stabilize derived phenoxyl radicals, model the covalent Y272–C228 linkage in GAO, and tune electronic effects, respectively. It is important to note that the foundation for the use of TACN–phenolate ligands in Cu(II) GAO modeling chemistry was laid by the early observation by Wieghardt and coworkers of photooxidation of a phenolate to a coordinated phenoxyl radical in Fe(III) complexes of a tris(phenolato)TACN ligand [46].

Upon deprotonation of the desired number of phenol units, a large number of mono- and bis-phenolate Cu(II) compounds have been isolated (**36**–**56**, Tables 4 and 5) [47–52]. In many cases, complexes of these ligands were also prepared with the non-redox active, spectroscopically innocent Zn(II) ion in order to assist in making spectral assignments [50,52,53]. Many of the complexes were characterized by X-ray crystallography and some representative Cu(II) structures are shown in Fig. 12. Typically, the compounds are five-coordinate with a slightly distorted square pyramidal geometry, although a coordination number of six was achieved by the addition of exogenous bidentate, monoanionic donors (**47** and **48**). In all of the Cu(II)–monophenolate derivatives (Table 4), as well as those such as **49** (Fig. 12b) that have bis(phenolato) ligation (Table 5), the phenolate donors reside in the equatorial plane at relatively short distances (Cu–O  $\sim$  1.85–1.95 Å), *cis* to either the exogenous donor group (mono-phenolates) or the second phenolate donor

Table 4

Summary of selected properties of Cu(II)–TACN complexes of  $[L^2]^-$  (where  $HL^2$  = phenol-containing TACN ligand shown in Fig. 11a)

No.	Formula	R <sub>1</sub>	R <sub>2</sub>	R <sub>3</sub>	UV–vis $\lambda_{\text{max}}$ , nm ( $\epsilon$ , M <sup>-1</sup> cm <sup>-1</sup> ) <sup>a</sup>	EPR <sup>b</sup>	CV <sup>c</sup>	Ref.
36	L <sup>2</sup> CuCl <sup>d</sup>	<i>i</i> -Pr	Me	Me	340 (3100), 520 (1500), 710 (sh, 440)	$g_{\parallel} = 2.25$ , $g_{\perp} = 2.03$ , $A_{\parallel} = 160$	$g_{\text{h}}$	[48]
37	L <sup>2</sup> CuCl	<i>i</i> -Pr	<i>t</i> -Bu	<i>t</i> -Bu	350 (3000), 526 (1200), 720 (sh, 400)	$g_{\parallel} = 2.26$ , $g_{\perp} = 2.04$ , $A_{\parallel} = 161$	$E_{1/2} = 0.59$ , $\Delta E_p = 86$	[48]
38	L <sup>2</sup> Cu(CF <sub>3</sub> SO <sub>3</sub> )	<i>i</i> -Pr	<i>t</i> -Bu	<i>t</i> -Bu	328 (3300), 532 (1100), 696 (sh, 450)	$g_{\parallel} = 2.25$ , $g_{\perp} = 2.03$ , $A_{\parallel} = 159$	$E_{1/2} = 0.72$ , $\Delta E_p = 96$	[48]
39	L <sup>2</sup> CuCl	<i>i</i> -Pr	Me	OMe	528 (1150) <sup>f</sup>	$g_{\parallel} = 2.26$ , $g_{\perp} = 2.02$ , $A_{\parallel} = 158$	$g_{\text{h}}$	[50]
40	L <sup>2</sup> CuCl·H <sub>2</sub> O	<i>i</i> -Pr	<i>t</i> -Bu	SMe	530 (950) <sup>f</sup>	$g_{\parallel} = 2.26$ , $g_{\perp} = 2.06$ , $A_{\parallel} = 157$	$E_{1/2} = 0.51$ , $\Delta E_p = 82$	[50]
41	L <sup>2</sup> CuOAc	<i>i</i> -Pr	<i>t</i> -Bu	<i>t</i> -Bu	474 (960) <sup>f</sup>	$g_{\parallel} = 2.26$ , $g_{\perp} = 2.03$ , $A_{\parallel} = 175$	$g_{\text{h}}$	[50]
42	L <sup>2</sup> CuOAc	<i>i</i> -Pr	Me	OMe	486 (900) <sup>f</sup>	$g_{\parallel} = 2.27$ , $g_{\perp} = 2.04$ , $A_{\parallel} = 167$	$g_{\text{h}}$	[50]
43	L <sup>2</sup> CuOAc <sup>d</sup>	<i>i</i> -Pr	Me	SMe	484 (810) <sup>f</sup>	$g_{\parallel} = 2.27$ , $g_{\perp} = 2.02$ , $A_{\parallel} = 166$	$g_{\text{h}}$	[50]
44	[L <sup>2</sup> Cu(CH <sub>3</sub> CN)]-(CF <sub>3</sub> SO <sub>3</sub> ) <sup>d</sup>	<i>i</i> -Pr	<i>t</i> -Bu	<i>t</i> -Bu	342 (3600), 538 (1440), 660 (sh, 700)	$g_{\parallel} = 2.25$ , $g_{\perp} = 2.03$ , $A_{\parallel} = 160$	$E_{1/2} = 0.79$ , $\Delta E_p = 92$	[50]
45	L <sup>2</sup> CuCl	Me	OMe	<i>t</i> -Bu	252 (8100), 315 (5300), 532 (1200)	$g_z = 2.24$ , $g_y = 2.05$ , $g_x = 2.05$ $A_z = 180$ , $A_x = A_y = 20$	$E_{1/2} = 0.45$ <sup>i</sup>	[51]
46	L <sup>2</sup> Cu(OCH <sub>2</sub> Ph) <sup>d</sup>	<i>i</i> -Pr	<i>t</i> -Bu	<i>t</i> -Bu	436 (700), 760 (130)	$g_z = 2.26$ , $g_y = 2.03$ , $g_x = 2.02$ $A_z = 161$	$E_{p,a} = 0.37$ <sup>h</sup>	[48]
47	L <sup>2</sup> Cu(Ph <sub>2</sub> acac) <sup>d,e</sup>	Me	OMe	<i>t</i> -Bu	254 (27100), 334 (16700), 358 (16400)	$g_z = 2.26$ , $g_y = 2.06$ , $g_x = 2.05$ $A_z = 176$ , $A_x = A_y = 21.7$	$E_{1/2} = 0.13$ <sup>i</sup>	[51]
48	L <sup>2</sup> Cu( <i>t</i> -Bu <sub>2</sub> acac) <sup>e</sup>	Me	OMe	<i>t</i> -Bu	256 (16000), 293 (18000), 451 (500)	$g_z = 2.25$ , $g_y = 2.07$ , $g_x = 2.06$ $A_z = 175$	$E_{1/2} = 0.04$ <sup>i</sup>	[51]

<sup>a</sup> All spectra in CH<sub>2</sub>Cl<sub>2</sub>, except complexes **44** (10:1 CH<sub>2</sub>Cl<sub>2</sub>/CH<sub>3</sub>CN) and **46** (THF).<sup>b</sup> Data obtained at X-band frequency, with  $A$  values in units of 10<sup>-4</sup> cm<sup>-1</sup>. For complexes **36–43** and **46** the solvent was 1:1 CH<sub>2</sub>Cl<sub>2</sub>/toluene; for complexes **45**, **47** and **48** the solvent was CH<sub>2</sub>Cl<sub>2</sub>; for complex **44** the solvent was 1:1:0.1 CH<sub>2</sub>Cl<sub>2</sub>/toluene/CH<sub>3</sub>CN.<sup>c</sup> Potentials reported in V and  $\Delta E_p$  values reported in mV. All processes are reversible unless otherwise noted. Experiments were performed in either CH<sub>2</sub>Cl<sub>2</sub> (complexes **36–45**, **47**, **48**) or CH<sub>3</sub>CN (complex **46**), with (Bu<sub>4</sub>N)PF<sub>6</sub> supporting electrolyte, and referenced vs. SCE. See individual references for specific details.<sup>d</sup> X-ray crystallography data has been reported.<sup>e</sup> acac<sup>-</sup> = acetylacetonate.<sup>f</sup> Additional intensity is present at longer wavelengths (~600–800 nm), but no bands are clearly resolved.<sup>g</sup> Potential not reported.<sup>h</sup> Irreversible process.<sup>i</sup> Corrected value, see Ref. [42] for details.

Table 5

Summary of selected properties of Cu(II)–TACN complexes of H<sub>2</sub>L<sup>3</sup> and H<sub>3</sub>L<sup>4</sup> (ligands shown in Fig. 11b and c, respectively)

No.	Formula	R <sub>1</sub>	R <sub>2</sub>	UV–vis $\lambda_{\text{max}}$ , nm ( $\epsilon$ , M <sup>−1</sup> cm <sup>−1</sup> ) <sup>a</sup>	EPR <sup>b</sup>	E-chem <sup>c</sup>	Ref.
49	L <sup>3</sup> Cu·MeOH <sup>d</sup>	<i>i</i> -Pr	<i>t</i> -Bu	300 (18000), 448 (1800), 706 (430)	$g_{\parallel} = 2.25$ , $g_{\perp} = 2.03$ , $A_{\parallel} = 169$	$E_{1/2}(1) = 0.50$ , $E_{1/2}(2) = 0.78$ , $\Delta E_p(1) = 93$ , $\Delta E_p(2) = 99$	[50]
50	L <sup>3</sup> Cu·0.5 CH <sub>2</sub> Cl <sub>2</sub> <sup>d</sup>	Et	OMe	252 (14500), 314 (22000), 458 (1450), 698 (210) <sup>e</sup>	$g_z = 2.243$ , $g_y = 2.052$ , $g_x = 2.051$ $A_z = 177$ , $A_x = A_y = 18$	$E_{1/2}(1) = 0.36$ , $E_{1/2}(2) = 0.60$ <sup>g</sup>	[52]
51	[HL <sup>3</sup> Cu]ClO <sub>4</sub>	Et	OMe	235 (12000), 296 (7500), 312 (7300) <sup>e</sup>	$g_z = 2.23$ , $g_y = 2.07$ , $g_x = 2.06$ $A_z = 155$ , $A_x = A_y = 10$	$E_{1/2} = 0.60$ <sup>g</sup>	[52]
52	HL <sup>4</sup> Cu	<i>t</i> -Bu	–	256 (17000), 288 (12000), 300 (12500), 305 (sh, 11000), 348 (sh), 428 (1100), 694 (br, 230)	$g_z = 2.24$ , $g_y = 2.05$ , $g_x = 2.06$ $A_z = 205$ , $A_x = A_y = 10$	$E_{1/2}(1) = 0.55$ , $E_{1/2}(2) = 0.78$ <sup>g</sup>	[49]
53	HL <sup>4</sup> Cu·MeOH <sup>d</sup>	OMe	–	236 (16000), 254 (12000), 297 (13000), 326 (sh), 445 (1500), 680 (br, 300)	$g_z = 2.25$ , $g_y = 2.05$ , $g_x = 2.06$ $A_z = 202$ , $A_x = A_y = 10$	$E_{1/2}(1) = 0.34$ , $E_{1/2}(2) = 0.52$ <sup>g</sup>	[49]
54	[H <sub>2</sub> L <sup>4</sup> Cu]ClO <sub>4</sub>	<i>t</i> -Bu	–	280 (14000), 321 (1700), 707 (sh), 822 (sh)	$g_z = 2.25$ , $g_y = 2.05$ , $g_x = 2.06$ $A_z = 174$ , $A_x = A_y = 14$	$E_{1/2} = 0.90$ <sup>g</sup>	[49]
55	[H <sub>2</sub> L <sup>4</sup> Cu]ClO <sub>4</sub>	OMe	–	293 (17000), 321 (sh), 565 (br, 1200)	$g_z = 2.24$ , $g_y = 2.06$ , $g_x = 2.07$ $A_z = 171$ , $A_x = A_y = 17$	$E_{1/2} = 0.72$ <sup>g</sup>	[49]
56	[H <sub>2</sub> L <sup>4</sup> Cu]ClO <sub>4</sub> <sup>d</sup>	H	–	279 (15000), 293 (12000), 320 (5420), 450 (1050), 581 (1040), 670 (390)	<sup>f</sup>	<sup>h</sup>	[47]

<sup>a</sup> All spectra in CH<sub>2</sub>Cl<sub>2</sub>, except complexes **52**, **53**, and **56** (CH<sub>3</sub>CN).<sup>b</sup> Data obtained at X-band frequency, with  $A$  values in units of 10<sup>−4</sup> cm<sup>−1</sup>. For complexes **50–55** the solvent was CH<sub>2</sub>Cl<sub>2</sub>; for complex **49** the solvent was 1:1 CH<sub>2</sub>Cl<sub>2</sub>/toluene.<sup>c</sup> Potentials reported in V and  $\Delta E_p$  values reported in mV. All processes are reversible unless otherwise noted. Experiments were performed in either CH<sub>2</sub>Cl<sub>2</sub> (complexes **49–51**, **54**, **55**) or CH<sub>3</sub>CN (complexes **52** and **53**) with (Bu<sub>4</sub>N)PF<sub>6</sub> supporting electrolyte, and referenced vs. SCE. See individual references for specific details.<sup>d</sup> X-ray crystallography data has been reported.<sup>e</sup> 0.1 M TBAPF<sub>6</sub>.<sup>f</sup> EPR data not reported.<sup>g</sup> Corrected value(s), see Ref. [42] for details.<sup>h</sup> CV not reported.

(bis-phenolates). Also, a significant elongation in the axial Cu–N bond is generally observed (typical Cu–N distance  $\geq 2.3$  Å).

The monophenolate complex **43** (Fig. 12a) is just one of several structurally analogous derivatives that differ only with respect to the identity of the fifth

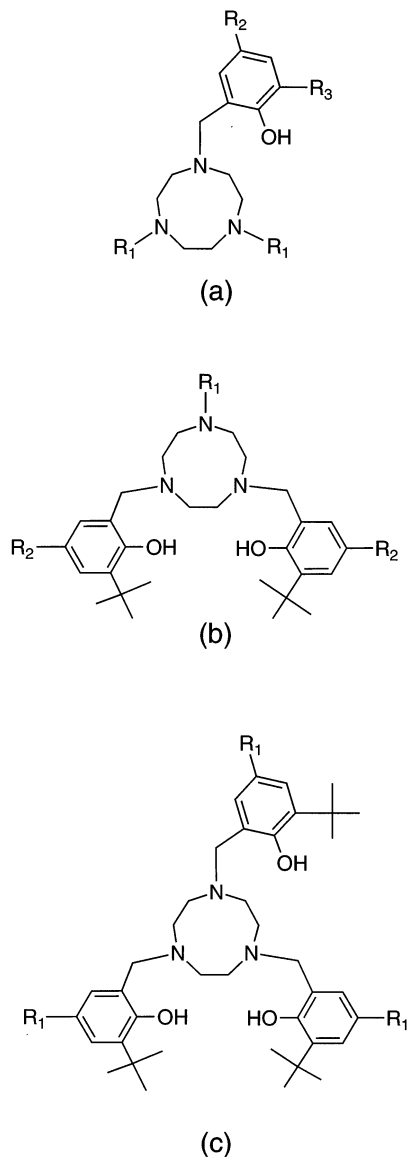


Fig. 11. General representations of the TACN ligands with (a) one phenol ( $\text{HL}^2$ ); (b) two phenol ( $\text{H}_2\text{L}^3$ ); and (c) three phenol ( $\text{H}_3\text{L}^4$ ) groups ( $\text{R}_1 = \text{R}_2 = \text{R}_3 =$  alkyl substituents).

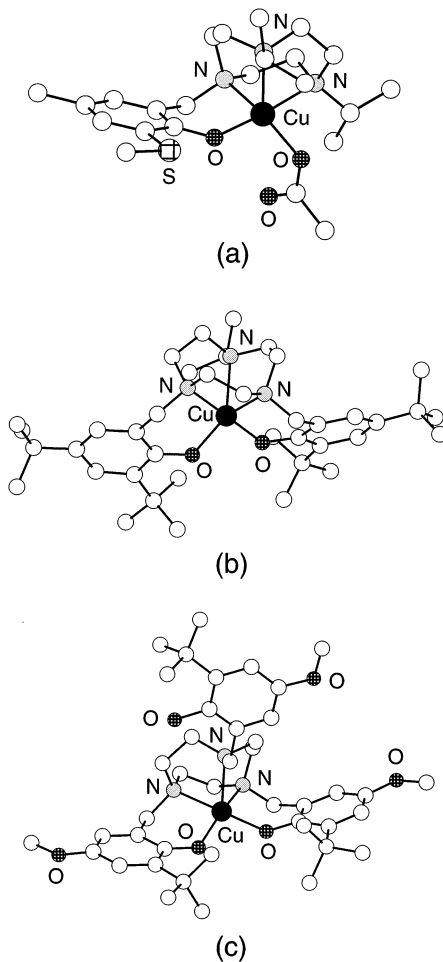


Fig. 12. X-ray crystal structures of the Cu(II)–phenolate complexes (a) **43** [50]; (b) **49** [50]; and (c) **53** [49].

exogenous donor ligand and/or phenolate substituents (Table 4). It is of particular interest due to its close structural similarity to the crystallographically characterized (pH 4.5) inactive form of GAO. Key replicative features include acetate coordination and an *ortho*-thioether containing phenolate group.

Complex **53** (Fig. 12c) has a third phenol group which remains uncoordinated; its coordination geometry closely resembles that of **49**. It should be noted that in complexes of these tris(phenolato) ligands with trivalent metal ions, ligation of all three phenolates occurs with extraordinarily high binding constants ( $K > 10^{30}$ ) [54,55]. Protonation of complexes like **53** leads to the formation of five-coordinate Cu(II)(phenol)(phenolate) complexes (e.g. **54–56**), where the equatorial phenol

group still interacts with the metal center [47,49]. While crystallographic data for **54** and **55** are not available, the structure of **56** has been determined (schematically shown in Fig. 13). The expected weaker interaction of the equatorial phenol group with Cu(II) is indicated by the Cu–O(phenol) bond length (2.09 Å) that is significantly longer than the Cu–O(phenolate) separation (1.83 Å). While this complex and those like it (**54** and **55**) accurately model the dual phenol/phenolate ligation proposed for the structure of Inactive GAO, the disposition of the donors (both equatorial) is different from that seen in the enzyme (one axial, one equatorial).

Many of the TACN-supported Cu(II)–phenolate complexes also have been characterized by EPR, UV–vis, and, in a few instances, resonance Raman spectroscopy (Tables 4 and 5). X-band EPR spectra generally contain axial signals (with minor rhombic components in some cases) consistent with a  $d^9$  Cu(II) ion in a square pyramidal geometry with a  $d_{x^2-y^2}$  ground state. All mono- and bis(phenolate) TACN Cu(II) complexes are also characterized by both phenolate  $\rightarrow$  Cu(II) CT ( $\lambda_{\text{max}} \approx 430\text{--}540$  nm,  $\epsilon \approx 1000\text{--}2000$  M $^{-1}$  cm $^{-1}$ ) and weak d–d ( $\lambda \approx 650\text{--}750$  nm,  $\epsilon \leq 750$  M $^{-1}$  cm $^{-1}$ ) bands in their absorption spectra. A typical spectrum (for **44**) is shown in Fig. 14 [50]. Consistent with the assignment of the higher energy transition as the phenolate  $\rightarrow$  Cu(II) CT, the location of this band was found to be sensitive to both the phenolate substituents and the nature of the second ligand (e.g. Cl $^{-}$  or OAc $^{-}$  vs. second phenolate or phenol). Increasing the electron donating ability of the phenolate ring substituents led to a bathochromic shift of the  $\lambda_{\text{max}}$ , consistent with an increase in the energy of filled phenolate-based orbitals. It should be noted that in cases where the electron-donating substituent is located in the *ortho* position (compare **40** to **37**, Table 4) the effect is not as significant as when the electron-donating substituent is located in the *para* position (compare **53** to **52**, Table 5). Addition of a second phenolate donor in place of the exogenous fifth

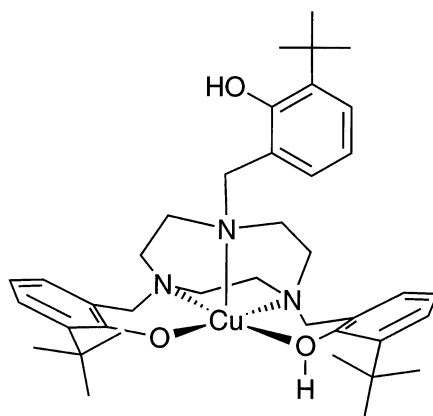


Fig. 13. Schematic representation of the structure of the mixed Cu(II)–phenolate/phenol complex **56** [47,49].

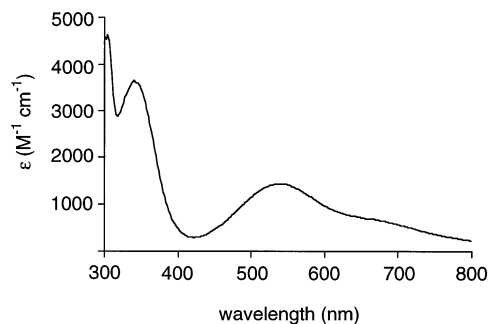


Fig. 14. Optical absorption spectrum of the Cu(II)–phenolate complex **44** in  $\text{CH}_2\text{Cl}_2$ .

ligand found in the mono-phenolate complexes significantly increases the energy of this transition (compare **49** to **37** and/or **53** to **45**), consistent with raised metal acceptor orbital energies. In selected cases, assignment of the 430–540 nm bands as phenolate  $\rightarrow$  Cu(II) CT transitions was supported by resonance Raman spectroscopy. Excitation into this absorption led to enhancements in high frequency bands associated with the metal–phenolate unit. For example, for **44** [50] peaks were seen at 1282 and 1605  $\text{cm}^{-1}$  that correspond to vibrational modes typically enhanced in Raman spectra of metal–tyrosinate units ( $\nu_{7a}$ , C–O stretch, and  $\nu_{8a}$ , ring deformation) [56,57]. These values closely match those observed for Inactive GLO (1267 and 1596  $\text{cm}^{-1}$ , respectively) [5].

The viability of coordinated Cu(II)–phenoxyl radical complexes derived from the Cu(II)–phenolate precursors discussed above was assessed by cyclic voltammetry. In all cases where benzylic C–H bonds are present in the phenolate donor (e.g. complexes **36**, **39**, **42**, and **43**) only irreversible oxidative processes were observed. These findings were attributed to the decomposition due to radical spin delocalization onto the reactive benzylic positions. On the other hand, if more resistive groups were incorporated into the *ortho* and *para* phenolate positions (e.g. *t*-butyl) fully reversible processes were seen for each coordinated phenolate donor. The  $E_{1/2}$  values (Tables 4 and 5) are similar to those of the mono- and bis(pyridyl)alkylamine complexes discussed in Sections 3.1 and 3.2. Controlled potential bulk electrolysis experiments showed that each oxidative process corresponds to removal of a single electron per phenolate ligand for the Cu(II) complexes. Essentially identical behavior was observed for a number of Zn(II) analogs, proving that these oxidative processes are ligand based, resulting in Cu(II)– and Zn(II)–phenoxyl radical complexes [50,52,53]. This assignment was further supported by UV–vis, EPR and resonance Raman spectroscopy (vide infra). The  $E_{1/2}$  values of the ligand-based oxidations were perturbed upon variation of the phenolate substituents. Thus, replacement of a *para* *t*-butyl group with a OMe group (**52**–**53**) led to a  $\Delta E_{1/2} = +210$  mV [49], but a smaller effect was seen in going from an *ortho* *t*-butyl to a SMe substituent (**37**–**40**,  $\Delta E_{1/2} = 50$  mV) [50]. This minor effect of an *ortho*-thioether on the Cu(II)–phenolate/Cu(II)–phenoxyl radical redox potential in these synthetic

models suggests that additional factors should be considered in explaining the low potential seen in GAO.

The electrochemical properties of the Cu(II)(phenol)(phenolate) complexes (**51**, **54**, **55**) were also explored [49,52]. In all cases only a single reversible process was observed, corresponding to the oxidation of the coordinated phenolate ligand. It is interesting to note that phenolate oxidation in these cases occurs at higher potential than for the unprotonated analogs with identical ring substituents (e.g. **54** vs. **52**,  $\Delta E_{1/2} = 350$  mV). Decreased electron density on the metal center upon protonation of the equatorial phenolate rationalizes this result. Additional oxidation of the coordinated or uncoordinated phenol moieties in these compounds was not reported.

Mono- and bis(phenoxyl radical) complexes of Cu(II) and Zn(II) were prepared on a larger scale by chemical or electrochemical oxidation of those phenolate compounds that exhibited reversible behavior in their cyclic voltammograms. In most cases this was done at low temperature (ca.  $-40^{\circ}\text{C}$ ) due to decomposition of the products under ambient conditions; an exception is a Zn(II) species that was isolated as a stable solid [53]. Despite the general temperature sensitivity of the metal–radical compounds, they were characterized extensively by spectroscopic methods. These studies of Cu(II) and Zn(II) systems [48–53], in combination with others focused on other transition metals [46,58], provided important insights into the structure and properties of the metal–phenoxyl radical unit. The discussion below will focus only on the spectroscopic features of Cu(II) complexes with a single coordinated phenoxyl radical which are most relevant to Active GAO.

In most cases, the Cu(II)–phenoxyl radical complexes proved to be EPR silent, indicative of antiferromagnetic coupling between the Cu(II)  $d_{x^2-y^2}$  orbital with the half filled  $\pi$  molecular orbital of the phenoxyl radical. However, oxidation of **47** (Fig. 15) and **48** (Table 4) resulted in the formation of Cu(II)–phenoxyl radical species that were EPR active. Triplet spectra were observed, consistent with ferromagnetic coupling between the phenoxyl radical and Cu(II); from analysis of

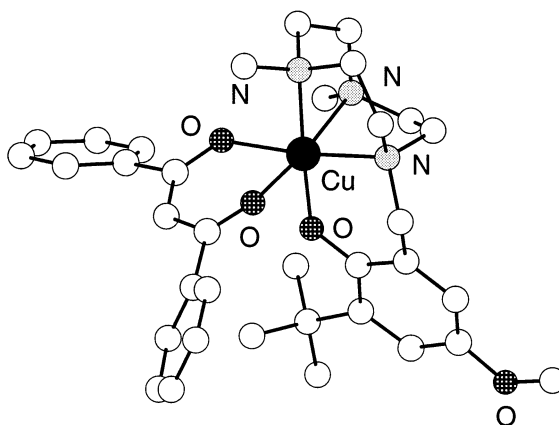


Fig. 15. X-ray crystal structure of the six-coordinate Cu(II)–phenolate complex **47** [51].

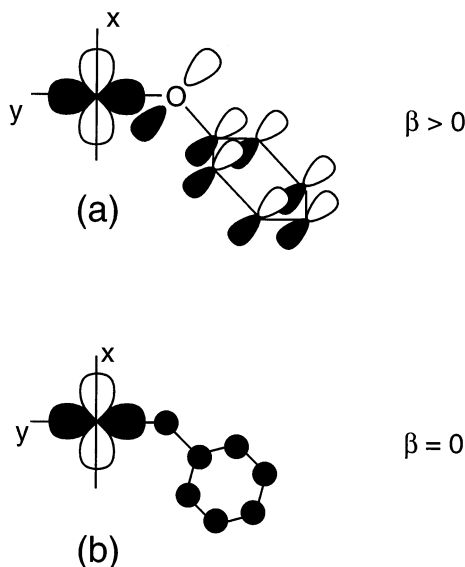


Fig. 16. Selected orientations of the Cu(II)  $d_{x^2-y^2}$  orbital and phenoxyl radical  $\pi$  molecular orbital in Cu(II)–phenoxyl radical complexes where  $\beta$  is the dihedral angle between the arene plane of the phenoxyl radical and the  $x,y$  plane of the Cu(II) ion. (a)  $\beta = 90^\circ$ , which leads to significant orbital overlap. (b)  $\beta = 0^\circ$ , which leads to no orbital overlap. In both drawings, the Cu–O–C angle  $\alpha$  is  $\sim 130^\circ$ ; for a discussion of how this angle is important in determining orbital overlap, see Ref. [51].

variable temperature data  $J = 16 \pm 3 \text{ cm}^{-1}$  ( $H = -2JS_1S_2$ ). Wieghardt and coworkers rationalized these divergent magnetic properties by a simple magnetostructural argument that centers on the magnitude of the dihedral angle  $\beta$  between the arene plane of the phenoxyl radical and the plane of the Cu  $d_{x^2-y^2}$  ground state orbital (Fig. 16). In **47**, which upon oxidation affords an EPR-active species, the value of  $\beta$  is about  $10^\circ$  smaller than that of **37** ( $17.6$  vs.  $27.4^\circ$ ), an example of a five-coordinate complex that yields an EPR silent product upon oxidation. This decrease in  $\beta$  is suggested to lead to less effective overlap between the Cu  $d_{x^2-y^2}$  orbital and the critical phenoxyl radical  $\pi$  molecular orbital, thus resulting in a change of the sign of the magnetic coupling interaction. Similar factors could be responsible for the  $S = 0$  state observed in Active GAO, where  $\beta \approx 75^\circ$ .

The UV–vis absorption spectra of the Cu(II)–phenoxyl radical complexes were distinguishable from those of their Cu(II)–phenolate precursors (cf. Fig. 17). Of particular note is an intense feature with  $\lambda_{\text{max}} \approx 390\text{--}430 \text{ nm}$  ( $\epsilon \approx 3000\text{--}8000 \text{ M}^{-1} \text{ cm}^{-1}$ ) that is generally assigned as the phenoxyl  $\pi \rightarrow \pi^*$  transition on the basis of enhancements of radical ring Raman modes upon laser excitation (vide infra) [49,50,58d]. Additional absorption intensity was observed at longer wavelength ( $\lambda_{\text{max}} \approx 600\text{--}800 \text{ nm}$ ). The molar absorptivity of this band generally is less than  $1000 \text{ M}^{-1} \text{ cm}^{-1}$ , but higher intensities have been observed in cases where an additional phenolate ligand is present (e.g. **49** $^{•+}$  and **50** $^{•+}$ ; Table 5). A similar low

energy feature is exhibited by Active GAO, but in the protein it is more intense and occurs at longer wavelength (Table 1). Only recently has this absorption feature been mimicked accurately in a model system (Section 3.5).

Insight into the spectroscopic properties of the coordinated phenoxyl radical without interference from features due to the  $d^9$  Cu(II) ion were obtained from studies of Zn(II)–phenoxyl radical analogs [50,52,53]. The EPR spectra of these complexes exhibit a  $S = 1/2$  signal centered at  $g \approx 2.0$  similar to those for free phenoxyl radicals [59]. Coordination of the phenoxyl radical in these Zn(II) complexes was indicated by the nature of the hyperfine coupling to the benzylic hydrogen atom(s). Delocalization of the unpaired spin density onto additional coordinated phenolate rings was observed in some cases [53]. The UV–vis spectra of these Zn(II)–phenoxyl radical complexes contain one or two intense features with  $\lambda_{\text{max}} \approx 400$  nm ( $\epsilon \approx 2500\text{--}8500$  M $^{-1}$  cm $^{-1}$ ; the radical  $\pi \rightarrow \pi^*$  transition) as well as a less intense, broad absorption at longer wavelength ( $\lambda_{\text{max}} \approx 550\text{--}750$  nm,  $\epsilon < 400$  M $^{-1}$  cm $^{-1}$ ). This longer wavelength absorption is consistently less intense than those seen in the analogous Cu(II)–phenoxyl radical complexes discussed above, consistent with the absence of contributions from ligand field transitions. It should be noted that the absorption features are very similar to those reported for a Zn(II) complex which contains a pendant uncoordinated phenoxyl radical [60]. These data suggest that sole use of UV–vis spectroscopy for distinguishing phenoxyl radical binding to a metal ion is unwise.

Resonance Raman spectroscopy has been particularly useful for gaining insight into the structural and electronic properties of the metal–phenoxyl radical unit [46,49,50,51,53,58c–e]. Laser excitation into the  $\pi \rightarrow \pi^*$  UV–vis band ( $\sim 400$  nm) results in resonance Raman spectra very similar to those of free phenoxyl radicals [57,61], with two dominant features at  $\sim 1500$  cm $^{-1}$  ( $\nu_{7a}$ , predominantly C–O stretching) and  $\sim 1600$  cm $^{-1}$  ( $\nu_{8a}$ ,  $C_{\text{ortho}}\text{--}C_{\text{meta}}$  ring stretching) (Table 6). The  $\nu_{7a}$  band in these complexes occurs at  $\sim 250$  cm $^{-1}$  higher energy than in the metal–phenolate precursors, indicative of increased C–O double bond character in the

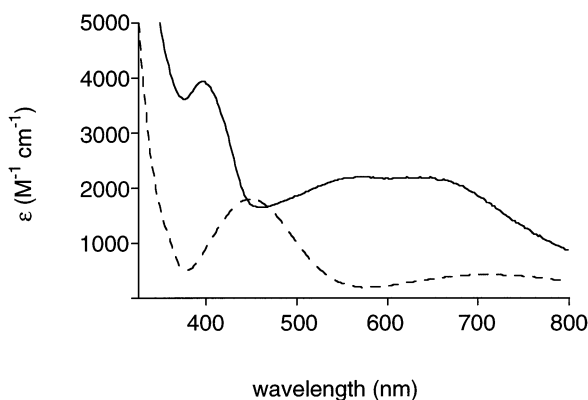


Fig. 17. Optical absorption spectra of **49** in CH<sub>2</sub>Cl<sub>2</sub> (---) and **49** $^{\bullet+}$  (—) that is formed upon oxidation with one equivalent of Ce(IV) in 1:0.1 CH<sub>2</sub>Cl<sub>2</sub>/CH<sub>3</sub>CN at  $-40^\circ\text{C}$  [50].

Table 6

Selected resonance Raman data for organic phenoxyl radicals and Cu–TACN phenoxyl radical complexes (TACN ligands shown in Fig. 11)

Compound	$\nu_{8a}$ (cm <sup>-1</sup> )	$\nu_{7a}$ (cm <sup>-1</sup> )	$\Delta$ (cm <sup>-1</sup> ) <sup>a</sup>	$\lambda_{ex}$ (nm)	Ref.
Phenoxyl	1557	1505	52	245	[57] <sup>i</sup>
Tyrosyl	1566	1510	55	245	<sup>j</sup>
2,6-Di- <i>t</i> -butyl-4-methoxyphenoxyl	1590	1511	79	413	[49]
(L <sup>2</sup> Cu) <sup>•+</sup> <sup>b</sup> ( <b>44</b> <sup>•+</sup> )	1600 <sup>h</sup>	1497	103	457.9	[50]
(L <sup>2</sup> Cu) <sup>•+</sup> <sup>c</sup> ( <b>48</b> <sup>•+</sup> )	1602	1509	107	413	[51]
(L <sup>3</sup> Cu) <sup>•+</sup> <sup>d</sup> ( <b>49</b> <sup>•+</sup> )	1599 <sup>h</sup>	1495	104	457.9	[50]
(HL <sup>4</sup> Cu) <sup>•+</sup> <sup>e</sup> ( <b>52</b> <sup>•+</sup> )	1590	1497	93	420	[49]
(HL <sup>4</sup> Cu) <sup>•+</sup> <sup>f</sup> ( <b>53</b> <sup>•+</sup> )	1614	1497	117	425	[49]
(H <sub>2</sub> L <sup>4</sup> Cu) <sup>•+</sup> <sup>g</sup> ( <b>54</b> <sup>•+</sup> )	1620	1494	126	430	[49]
Active GAO	1595	1487	108	875	[16]

<sup>a</sup>  $\Delta = \nu_{8a} - \nu_{7a}$ .

<sup>b</sup> R<sub>1</sub> = *i*-Pr; R<sub>2</sub> = R<sub>3</sub> = *t*-Bu.

<sup>c</sup> R<sub>1</sub> = Me; R<sub>2</sub> = OMe; R<sub>3</sub> = *t*-Bu.

<sup>d</sup> R<sub>1</sub> = *i*-Pr; R<sub>2</sub> = *t*-Bu.

<sup>e</sup> R<sub>1</sub> = *t*-Bu.

<sup>f</sup> R<sub>1</sub> = OMe.

<sup>g</sup> R<sub>1</sub> = *t*-Bu.

<sup>h</sup> Weak band.

<sup>i</sup> D.M. Chipman, R. Liu, X. Zhou, P. Pulay, J. Chem. Phys. 100 (1994) 5023.

<sup>j</sup> C.R. Johnson, M. Ludwig, S.A. Asher, J. Am. Chem. Soc. 108 (1986) 905.

coordinated phenoxyl radicals. This structural attribute has been corroborated by an X-ray crystal structure of a Cr(III)–phenoxyl radical complex [58a]. In this structure both a decrease in the C–O and the C<sub>ortho</sub>–C<sub>meta</sub> bond distances relative to its Cr(III)–phenolate redox isomer were observed, consistent with the semiquinonato resonance formulation being a major contributor in this instance (Fig. 18).

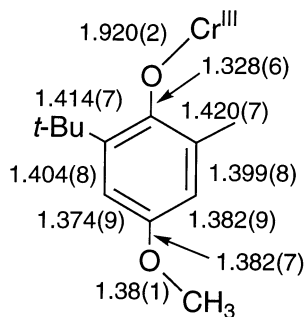
In addition, Wieghardt and coworkers found that both the relative locations and intensities of the  $\nu_{7a}$  and  $\nu_{8a}$  phenoxyl radical Raman bands are sensitive to metal coordination [58d]. In coordinated phenoxyl radical complexes, the difference between  $\nu_{8a}$  and  $\nu_{7a}$  ( $\Delta$ ) is always greater than 90 cm<sup>-1</sup> (cf. Cu cases listed in Table 6), with  $\nu_{8a}$  usually more intense than  $\nu_{7a}$ . In contrast, for uncoordinated phenoxyl radicals  $\Delta$  is always less than 80 cm<sup>-1</sup> and  $\nu_{7a}$  is the more intense vibration. Thus, resonance Raman spectroscopy offers a particularly useful method for distinguishing free from coordinated phenoxyl radicals.

Another TACN-supported complex of particular relevance to GAO is **46** (Fig. 19), in which a benzyl alcoholato ligand and a phenolate donor are coordinated in a *cis*-equatorial arrangement. Interestingly, a C–H $\cdots$ O hydrogen bonding interaction between a benzylic hydrogen and the phenolate oxygen is implicated by the X-ray crystallographic data (C $\cdots$ O = 2.995(3) Å). This structure mimics the proposed disposition of substrate and Y272 in GAO [25] (Fig. 3), with the observed H-bonding interaction foreshadowing H-atom abstraction by the (derived) phe-

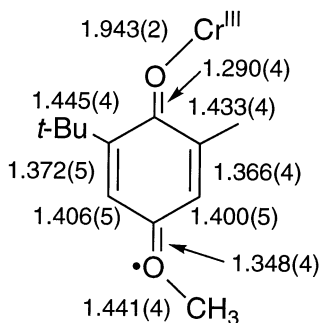
noxy radical during turnover. Indeed, oxidation of **46** results in interesting biomimetic reactivity (Section 4).

### 3.4. Complexes containing salen and reduced salen ligands

Bis(phenolate)–Cu(II) complexes which serve as models for GAO have been prepared utilizing substituted salen and reduced salen-type ligand frames (Fig. 20). Important features of these complexes include (i) the presence of steric bulk and limited ligand flexibility, which inhibits bis( $\mu$ -phenolate) dimer formation; and (ii) the ability to oxidize one of the phenolate arms to a phenoxyl radical when the aryl ring is properly protected. While a number of Cu(II)–salen complexes possess a square planar  $N_2O_2$  coordination geometry [62], it was discovered that significant tetrahedral distortion could be induced upon addition of bulky phenolate sub-



(a)



(b)

Fig. 18. Selected bond lengths for (a) Cr(III)–phenolate and (b) Cr(III)–phenoxyl radical units in complexes structurally characterized by X-ray crystallography [58a].

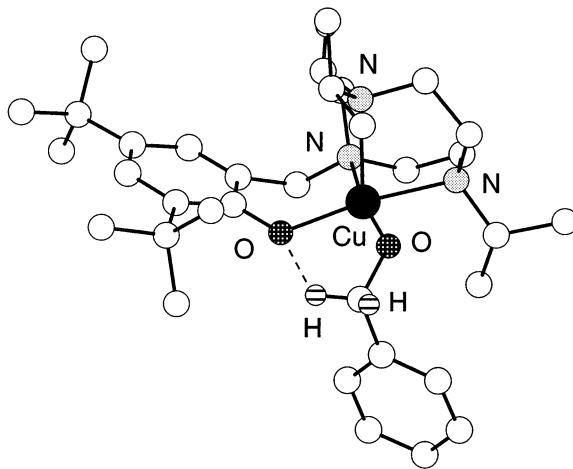


Fig. 19. X-ray crystal structure of the Cu(II)–alcoholato/phenolate complex **46** [48].

stituents (*vide infra*) and/or large ( $\geq 3$  carbon atoms) tethers between the diimine backbone [63–65].

All salen complexes shown in Table 7 (**57–65**) possess such a tetrahedral distortion, which has been suggested to be important in stabilizing Cu(I) forms of

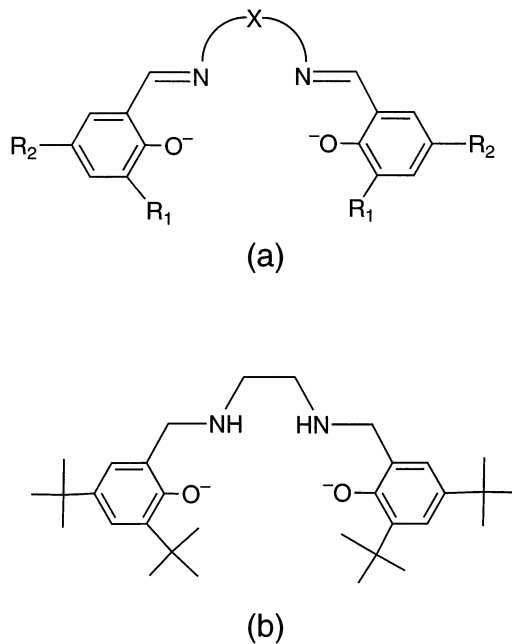


Fig. 20. (a) General representation of the bis(phenolate) salen ligands,  $[L^5]^{2-}$  ( $R_1 = R_2 =$  alkyl substituents). (b) Representation of a bis(phenolate) reduced-salen ligand.

Table 7  
Summary of selected properties of Cu(II)–salen complexes of  $[L^5]^{2-}$  (ligand shown in Fig. 20a)

No.	X	R <sub>1</sub>	R <sub>2</sub>	UV–vis $\lambda_{\text{max}}$ , nm ( $\epsilon$ , M <sup>−1</sup> cm <sup>−1</sup> ) <sup>a</sup>	EPR <sup>b</sup>	CV <sup>c</sup>	Ref.
57	1,3-(2-Hydroxypropyl)	H	H	370 (11300), 611 (263)	$g_{\parallel} = 2.247$ , $g_{\perp} = 2.053$ , $A_{\parallel} = 181$	<sup>c</sup>	[64]
58	1,2-Cyclohexyl	S- <i>i</i> Pr	<i>t</i> -Bu	<sup>d</sup>	$g_{\parallel} = 2.354$ , $g_{\perp} = 2.042$ , $A_{\parallel} = 212$ , $A_{\perp} = 31$	$E = 1.00$ <sup>f</sup>	[65a]
59	2,2'-Binaphthyl	S-Ph	<i>t</i> -Bu	420 (15000), 624 (500)	$g_{\parallel} = 2.191$ , $g_{\perp} = 1.994$ , $A_{\parallel} = 188$ , $A_{\perp} = 16$	$E = 1.00$	[65]
60	2,2'-Binaphthyl	S- <i>i</i> Pr	<i>t</i> -Bu	424 (13300), 641 (600)	$g_{\parallel} = 2.145$ , $g_{\perp} = 1.959$ , $A_{\parallel} = 193$ , $A_{\perp} = 12$	$E = 0.92$	[65]
61	2,2'-Binaphthyl	H	<i>t</i> -Bu	<sup>d</sup>	$g_{\parallel} = 2.41$ , $g_{\perp} = 2.012$ , $A_{\parallel} = 175$ , $A_{\perp} = 12$	$E = 1.08$	[65]
62	2,2'-Binaphthyl	S-Ph	H	<sup>d</sup>	$g_{\parallel} = 2.163$ , $g_{\perp} = 1.975$ , $A_{\parallel} = 195$ , $A_{\perp} = 12$	$E = 1.00$	[65]
63	2,2'-Binaphthyl	<i>t</i> -Bu	<i>t</i> -Bu	<sup>d</sup>	$g_{\parallel} = 2.215$ , $g_{\perp} = 2.047$ , $A_{\parallel} = 179$ , $A_{\perp} = 13$	$E_{1/2}(1) = 0.81$ , $\Delta E_p = 80$ , $E_{1/2}(1) = 0.98$ , $\Delta E_p = 67$ <sup>g</sup>	[65]
64	2,2'-Binaphthyl	H	H	<sup>d</sup>	$g_{\parallel} = 2.354$ , $g_{\perp} = 2.042$ , $A_{\parallel} = 212$ , $A_{\perp} = 31$	$E = 1.10$	[65]
65	2,2'-Binaphthyl	Br	Br	<sup>d</sup>	$g_{\parallel} = 2.242$ , $g_{\perp} = 2.059$ , $A_{\parallel} = 182$	<sup>c</sup>	[65b]

<sup>a</sup> Spectra recorded in DMF (**57**), CH<sub>3</sub>CN (**59**) or THF (**60**).

<sup>b</sup> Data obtained at X-band frequency, with A values in units of 10<sup>−4</sup> cm<sup>−1</sup>. For complexes **58–65** the solvent was 1:1 CH<sub>3</sub>CN/toluene; for complex **57** the solvent was CHCl<sub>3</sub>.

<sup>c</sup> Potentials reported in V and  $\Delta E_p$  values reported in mV. Process reversibility was not reported unless otherwise noted. Experiments were performed in CH<sub>3</sub>CN with (Bu<sub>4</sub>N)PF<sub>6</sub> supporting electrolyte, and referenced vs. SCE. See individual references for specific details.

<sup>d</sup> UV–vis data not reported.

<sup>e</sup> CV not reported.

<sup>f</sup> Estimated value.

<sup>g</sup> Reversible processes.

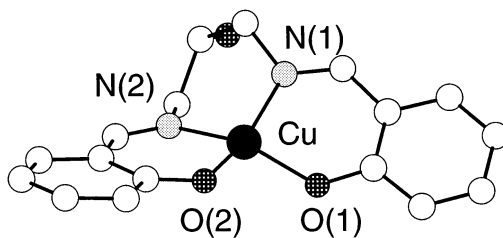


Fig. 21. X-ray crystal structure of the Cu(II)–salen complex **57** [64].

these complexes and facilitating substrate binding during biomimetic alcohol oxidation catalysis (*vide infra*) [65]. Illustrative X-ray crystal structures are shown in Figs. 21 and 22 [64,65a]. In both structures, a large dihedral angle between the planes O(1)–Cu–N(1) and O(2)–Cu–N(2) indicates the deviation from planarity (35.7 and 30°, respectively). Spectroscopic studies (Table 7) revealed UV–vis transitions consistent with a phenolate  $\rightarrow$  Cu(II) CT band and d–d transitions, the bis(imine) ligation apparently being responsible for the high extinctions seen for the former. Axial signals in EPR spectra corroborate  $d_{x^2-y^2}$  ground states for the compounds.

Complexes **58–65** are characterized by high potential oxidative processes in their cyclic voltammograms (0.81–1.0 V vs. SCE; Table 7) [65]. No clear relationship between the supporting ligand substituent pattern and the redox potential is evident. Addition of one equivalent of a strong oxidant (NOBF<sub>4</sub> or TPASbCl<sub>6</sub>) [66] to the complexes that possess both 3- and 5-substituents and a binaphthyl diimine linker (**59**, **60**, **63**, **65**) resulted in the quenching of their axial EPR signals, implicating the generation of room temperature stable, antiferromagnetically coupled coordinated phenoxyl radical species. X-ray absorption (XAS) and extended

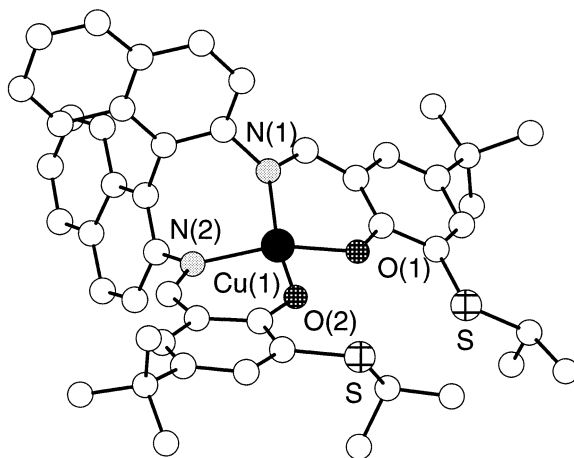


Fig. 22. X-ray crystal structure of the Cu(II)–salen complex **60** [65].

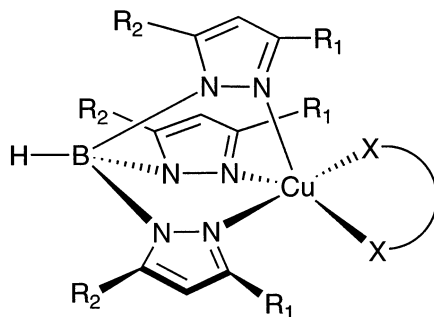


Fig. 23. Schematic representation of  $\text{Tp}^{\text{R}}\text{Cu(II)}(\text{phenolate})$  complexes, where X = an exogenous, bidentate phenolate ligand ( $\text{R}_1 = \text{R}_2 =$  alkyl substituents; see Table 8).

X-ray absorption fine-structure (EXAFS) data suggested that these  $\text{Cu(II)}$ –phenoxyl radical complexes (e.g.  $[\mathbf{63}]^{*+}$ ) are able to interact with anionic ligands to form species formulated as  $[(\mathbf{63})(\text{X})]^*$ , where  $\text{X} = \text{BF}_4^-$  or  $\text{OMe}^-$ . This result prompted the investigation of the reactivity of such complexes with alkoxides, potential alcohol oxidation substrates (*vide infra*). It is relevant in this regard that the isolation of a salen– $\text{Cu(I)}$  complex (with the ligand of **59**) was reported and it was invoked as a catalytic intermediate; however, little characterization data was provided [65b].

A final complex related to those discussed above (**66**) was constructed using the reduced salen ligand shown in Fig. 20b [67]. While X-ray crystal structure data was not reported, the complex is presumed to be square planar on the basis of EPR data as well as the increased flexibility characteristic of its diamine backbone (as opposed to the diimine complexes discussed above). This complex can be oxidized at  $-60^\circ\text{C}$  upon treatment with one equivalent of  $\text{Ce}(\text{NO}_3)_6(\text{NH}_4)_2$  in accordance with the reported electrochemical data for this complex. UV–vis and EPR data are consistent with the formation of a  $\text{Cu(II)}$ –phenoxyl radical complex ( $[\mathbf{69}]^{*+}$ ) upon oxidation.

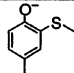
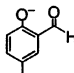
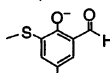
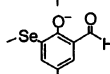
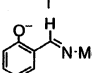
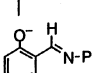
### 3.5. Complexes containing substituted hydrotris(pyrazolyl)borates

The hydrotris(pyrazolyl)borate ligand ( $\text{Tp}^{\text{R}}$ ) framework has been used previously in bioinorganic chemistry to bind to Cu, Fe, and Zn [68], in large part because it offers histidine-like N-donors and facile tunability of both steric and electronic properties upon variation of the pyrazolyl substituents. A key feature is the presence of two available coordination sites in  $\text{Tp}^{\text{R}}$  complexes of  $\text{Cu(II)}$  that may be filled with exogenous bidentate, phenolate-containing ligands. The resulting five-coordinate, square pyramidal  $\text{Cu(II)}$  complexes have been suggested to be structural models of GAO (Fig. 23, Table 8).

The first such example to be reported (**67**, Fig. 24) [69] is characterized by a phenolate  $\rightarrow \text{Cu(II)}$  CT band and a d–d transition in its UV–vis spectrum. The cyclic voltammogram revealed a single irreversible oxidative process at 1.07 V vs.

Table 8

Summary of selected properties of monomeric Cu(II)(Tp<sup>R</sup>)(phenolate) complexes (schematic shown in Fig. 23)

No.	R <sub>1</sub>	R <sub>2</sub>	phenolate	UV-vis	EPR <sup>b</sup>	CV <sup>c</sup>	ref.
				$\lambda_{\text{max}}$ , nm ( $\epsilon$ , M <sup>-1</sup> cm <sup>-1</sup> ) <sup>a</sup>			
67	cumenyl	Me		485 (1530), 756 (510)	<i>d</i>	$E_{\text{p,a}} = 1.07^e$	69
68	Ph	H		254 (sh), 313 (sh), 409 (3400), 427 (sh), 684 (93)	$g_{\parallel} = 2.284$ , $g_{\perp} = 2.065$ , $A_{\parallel} = 170$	$E_{\text{p,a}} = 1.30$	70
69	Ph	H		254 (sh), 319 (8200), 437 (4000), 685 (92)	$g_{\parallel} = 2.286$ , $g_{\perp} = 2.065$ , $A_{\parallel} = 174$	$E_{1/2} = 0.99^f$	70b
70	Ph	H		254 (sh), 290 (sh), 329 (5400), 441 (3900), 460 (sh), 669 (110)	$g_{\parallel} = 2.289$ , $g_{\perp} = 2.065$ , $A_{\parallel} = 175$	$E_{\text{p,a}} = 0.99$	70b
71	Ph	H		254 (sh), 309 (2700), 390 (5100), 642 (148)	$g_{\parallel} = 2.252$ , $g_{\perp} = 2.060$ , $A_{\parallel} = 189$	$E_{\text{p,a}} = 1.05$	70b
72	Ph	H		254 (sh), 295 (sh), 415 (3400), 664 (92)	$g_{\parallel} = 2.271$ , $g_{\perp} = 2.060$ , $A_{\parallel} = 180$	$E_{\text{p,a}} = 1.10$	70b

<sup>a</sup> All spectra in CH<sub>2</sub>Cl<sub>2</sub>, except complex 67 (toluene).

<sup>b</sup> Data obtained at X-band frequency in 10:1 CH<sub>2</sub>Cl<sub>2</sub>/toluene, with A values in units of 10<sup>-4</sup> cm<sup>-1</sup>.

<sup>c</sup> Potentials reported in V. All processes are irreversible unless otherwise noted. Experiments were performed in CH<sub>2</sub>Cl<sub>2</sub> with (Bu<sub>4</sub>N)PF<sub>6</sub> supporting electrolyte, unless otherwise noted and referenced vs. SCE. See individual references for specific details.

<sup>d</sup> EPR data not reported.

<sup>e</sup> Supporting electrolyte not reported. Potential corrected and referenced to SCE (see reference 42), based on the assumption that the supporting electrolyte was (Bu<sub>4</sub>N)PF<sub>6</sub>.

<sup>f</sup> Reversible process.

SCE that was attributed to phenolate oxidation and subsequent dissociation of the *ortho*-thioether. It is also conceivable that the presence of a potentially reactive *para* benzylic position may also facilitate the decomposition. The X-ray crystal structure revealed a coordination sphere made up of one axial pyrazole donor from  $\text{Tp}^{\text{Cum,Me}}$  as well as two pyrazole N donors, one phenolate O atom and an S donor from the 2-(methylsulfanyl) phenol moiety in the equatorial plane. A major difference between this model and those discussed previously is the thioether ligation in the final equatorial site. The short Cu–S bond distance (2.394 Å) indicates a strong interaction, and the thioether is believed to remain coordinated even in MeOH solutions. The authors speculate that Trp290 may play a role in discouraging thioether ligation into the substrate-binding site in GAO. Thus Trp290 is proposed to both lower the redox potential of Y272 via a  $\pi$ -stacking interaction (electronic effect) as well as inhibiting S coordination of Cys228 that would occur upon rotation of the Cys228-Tyr272 unit (steric effect).

A series of similar Cu(II) complexes incorporating a slightly less hindered  $\text{Tp}^{\text{R}}$  ligand in conjunction with either a substituted salicylaldehyde or phenol/Schiff base group also have been synthesized (Table 8) [70]. Many of these complexes have been structurally characterized; an example can be seen in Fig. 25. The overall coordination for each member of the series is quite similar to the one shown, but subtle changes in the equatorial plane geometries are observed, depending on the nature of the exogenous phenolate ligand. Complexes **68**–**72** are characterized by phenolate  $\rightarrow$  Cu(II) CT bands in their UV–vis spectra as well as axial signals in their EPR spectra (Table 8). Electrochemical experiments revealed one oxidative process in each case, which was attributed to ligand based oxidation to form Cu(II)–phenoxy radical complexes. Examination of the potential associated with these oxidative processes revealed that the presence of either an electron donating SMe or SeMe substituent in the *ortho* position led to a more facile oxidative process

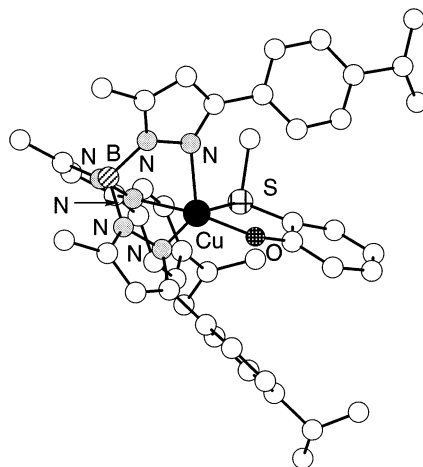


Fig. 24. X-ray crystal structure of the  $\text{Tp}^{\text{R}}\text{Cu(II)}(\text{phenolate})$  complex **67** [69].

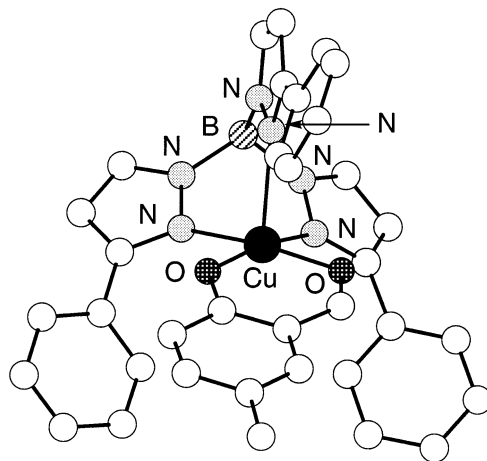


Fig. 25. X-ray crystal structure of  $\text{Tp}^{\text{R}}\text{Cu}(\text{II})(\text{phenolate})$  complex **68** [70].

(e.g. approximately 300 mV difference between **68** and **69**). Note that while this process is irreversible for complexes **68** and **70–72**, it is reversible for **69** even in the absence of a resistive group in the *para* phenolate position. The electrochemistry of **69** was further explored by controlled potential bulk electrolysis, which yielded a brown solution corresponding to  $[\mathbf{69}]^{*+}$ . If allowed to stand at ambient temperature the solution slowly decomposed ( $t_{1/2} = 10$  h), but if the oxidized solution was immediately reduced, **69** was regenerated in 90+ % yield, consistent with the reversible behavior seen by cyclic voltammetry. The oxidized product lacked an EPR signal, consistent with spin coupling between the  $d^9$  Cu(II) ion and the derived phenoxyl radical. The UV–vis spectrum revealed the expected phenoxyl radical  $\pi \rightarrow \pi^*$  transitions. In addition, absorptions with  $\lambda_{\text{max}} > 800$  nm were observed for the first time in synthetic model compounds; these features are similar to those seen in Active GAO. In Active GAO, the multiple long wavelength absorptions were attributed to a ligand–ligand charge transfer (LLCT) involving Y272 and Y495, but a similar transition is not possible in this case. This finding suggests that at least some of this intensity in the protein spectrum may be associated with some other process(es) involving the Y272· unit.

### 3.6. Complexes containing other supporting ligands

While the majority of GAO model complexes have made use of the ligand frameworks discussed above, a number of relevant complexes utilizing other supporting ligands also have been reported. For example, *ortho*-thioether or -sulfoxide phenolates were added to  $[\text{Cu}(\text{PMDT})(\text{CH}_3\text{CN})_2](\text{ClO}_4)_2$  (where PMDT = 1,1,4,7,7-pentamethyldiethylenetriamine) [71]. Five coordinate Cu(II)-complexes with the PMDT ligand occupying three coordination sites and the final two sites occupied by the bidentate exogenous phenolate donors (phenolate O and

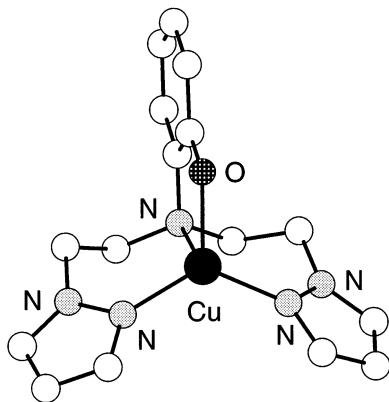


Fig. 26. X-ray crystal structure of the four-coordinate Cu(I)–phenolate complex **73** [73].

either thioether S or sulfoxide O atom) were isolated and structurally characterized. UV–vis and EPR spectra confirmed Cu(II)–phenolate complex formation.

Complexes serving as models for the Cu(I)-containing Reduced form of GAO also have been reported. While this form is proposed to contain a coordinated tyrosine residue (rather than a tyrosinate; Fig. 2), the models reported to this point contain coordinated phenolate donors [72]. In the first example, a monomeric Cu(I)–phenolate complex, **73**, was formed upon reaction of a bis(pyrazolyl)alkyl amine phenolate with  $[\text{Cu}(\text{CH}_3\text{CN})_4]\text{BF}_4$  [73]. The crystal structure of this complex (Fig. 26), revealed a Cu(I) ion in a distorted trigonal pyramidal geometry, ligated by an three N donors and one phenolate O atom. The average Cu–ligand bond length is 2.03 Å. While CO reactivity of this complex was investigated, reactions with molecular oxygen that would be relevant to the GAO catalytic cycle were not described.

Another relevant monomeric Cu(I)–phenolate complex is supported by a 1,5-diazacyclooctane (DACO) framework, with a single appended phenolate [74]. As seen

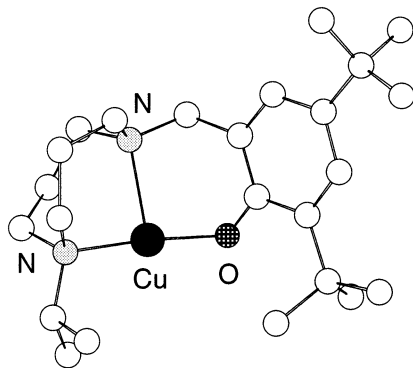


Fig. 27. X-ray crystal structure of three-coordinate Cu(I)–phenolate complex **74** [74].

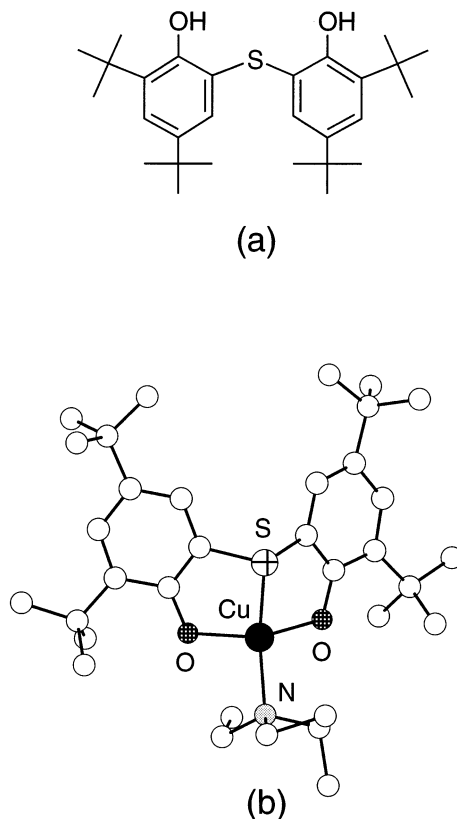


Fig. 28. (a) Representation of the bis(phenol)-thioether ligand,  $H_2L^6$ . (b) X-ray crystal structure of the Cu(II) complex **75** of  $[L^6]^{2-}$  [75].

in Fig. 27, **74** has a T-shaped coordination geometry about Cu, with an average Cu–ligand (O or N) bond length of 2.05 Å. The three-coordinate geometry and the bond distances closely model data for the Reduced GAO site [21]. Cyclic voltammetry performed on **74** revealed the presence of a reversible oxidative process at  $-0.10$  V versus SCE. Consistent with this low potential, **74** readily reacts with  $O_2$  at  $-78^\circ\text{C}$  to yield a metastable intermediate, characterized by a rich absorption spectrum and EPR silence. While assignment of this intermediate as a Cu/ $O_2$  species cannot be ruled out, the spectroscopic data are consistent with it being a Cu(II)–phenoxyl radical complex derived from two electron oxidation of the Cu(I)–phenolate precursor. Such a reaction is very similar to that of Reduced GAO with  $O_2$  (Fig. 3).

A recent study reported the use of a bis(phenol) thioether ligand ( $H_2L^6$ , Fig. 28a) as a supporting ligand for a Cu(II) complex which was found to be an alcohol oxidation catalyst (vide infra) [75]. Reaction of  $H_2L^6$  with CuCl and  $Et_3N$  in MeOH and subsequent exposure to  $O_2$  led to the formation of the bis(phenolate)thioether–Cu(II) complex (**75**) shown in Fig. 28b. This complex was found to be paramagnetic

( $\mu_{\text{eff}} = 1.79\mu_{\text{B}}$ ) and to exhibit two quasireversible one-electron oxidative processes in its cyclic voltammogram ( $E_{1/2} = 0.96$  and  $1.35$  V vs. SCE) corresponding to sequential phenoxyl radical generation. On the other hand, if the synthesis was carried out in THF, a different species was formed (**76**, Fig. 29). The complex is proposed to contain two four-coordinate Cu(II) ions, each ligated by one thioether S atom, one phenoxyl radical, and two bridging phenolate groups. The formulation of this Cu(II)–phenoxyl radical species is supported by an absorption spectrum similar to that of other Cu(II)–phenoxyl radical complexes ( $\lambda_{\text{max}} \approx 404$  nm,  $\epsilon = 8000$  M $^{-1}$  cm $^{-1}$ ), phenoxyl radical ring modes in resonance Raman spectra obtained using excitation into the  $\pi \rightarrow \pi^*$  transition (1451, 1579, 1594, and 1606 cm $^{-1}$ ), as well as the lack of an EPR signal consistent with coupling of all four spins in the complex. No X-ray crystal structure data for **76** is available.

Another recent study detailed the synthesis of a Cu(II)–iminosemiquinone complex as a model for Active GAO [76]. As discovered previously [77], the supporting ligand for these complexes ligand can exist in three different redox forms,  $[\text{L}^7]^{3-}$ ,  $[\text{L}^7]^{2-}$ ,  $[\text{L}^7]^{1-}$  (Fig. 30). A square planar Cu(II)–triethylamine adduct (**77**, Fig. 31) of  $[\text{L}^7]^{2-}$  was generated upon reaction of  $[\text{Cu}(\text{CH}_3\text{CN})_4]\text{ClO}_4$  with  $(\text{H}_4\text{L}^7)(\text{CF}_3\text{CO}_2)$  and  $\text{NEt}_3$  in  $\text{CH}_3\text{CN}$ , followed by exposure to air at ambient temperature. Consistent with the formulation of the supporting ligand as  $[\text{L}^7]^{2-}$ , **77** was found to be diamagnetic due to spin coupling of the  $d^9$  Cu(II) ion and the  $S = 1/2$  iminosemiquinone radical ( $J = -137$  cm $^{-1}$ ;  $H = -2JS_1S_2$ ). In addition, the cyclic voltammogram of **77** revealed two reversible, one electron ligand-based processes ( $E_{1/2}(1) = 0.32$  V,  $E_{1/2}(2) = -0.60$  V vs. SCE) corresponding to oxidation to form  $[\text{L}^7]^{1-}$  and reduction to form  $[\text{L}^7]^{3-}$ , respectively. While this system is different from Active GAO in that the organic radical is an iminosemiquinone and not a simple phenoxyl radical, overall a similar spin system to GAO was obtained, and this complex (**77**) was found to be an effective alcohol oxidation catalyst under quite mild conditions (vide infra).

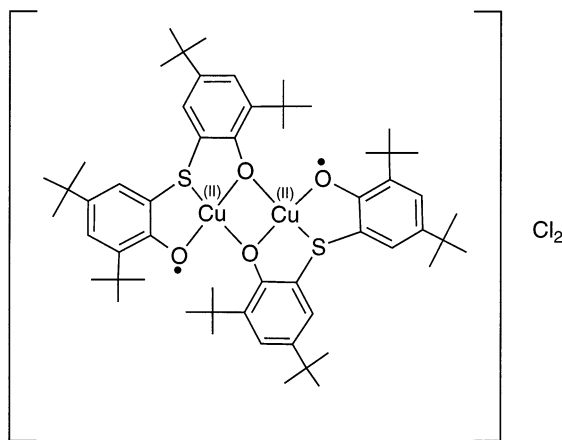
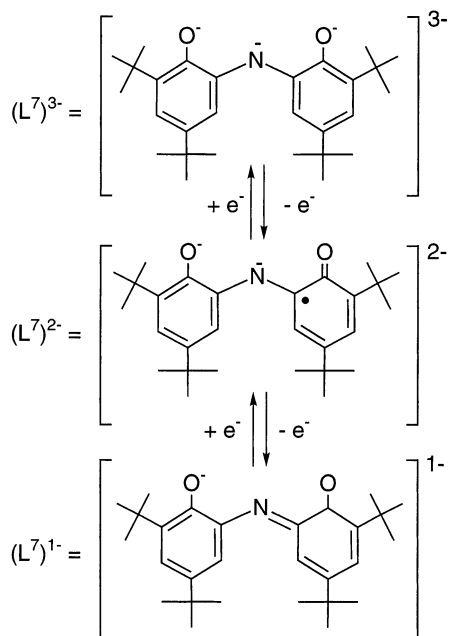
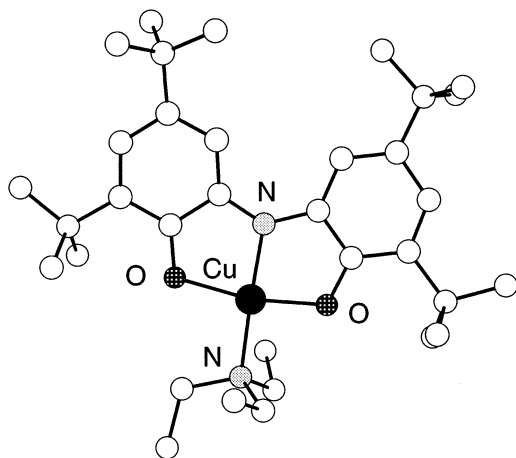


Fig. 29. Proposed structure for the catalyst **76** [75].

Fig. 30. Representation of the three different redox levels of  $L^7$ .

Upon reaction of a MeOH solution of **77** with excess  $H_2O_2$  at  $-80^\circ C$ , or upon reaction of  $[Cu(CH_3CN)_4]ClO_4$  with  $(H_4L^7)(CF_3CO_2)$  and  $NEt_3$  in MeOH followed by exposure to dry  $O_2$  at  $-50$  to  $-70^\circ C$ , a new species was formed (**78**). This species was formulated to be the Cu(II)–superoxo complex  $[Cu(H_2L^{7-})(O_2^{\bullet-})(NEt_3)]$  [78], an intriguing result considering that there is only one other example of

Fig. 31. X-ray crystal structure of the Cu(II) complex **77** of  $[L^7]^{2-}$  [76].

an isolated and well-characterized Cu(II)–superoxo species, a side-on Cu(II)–superoxo complex reported by Kitajima and coworkers [79]. Complex **78** exhibits a UV–vis spectrum with  $\lambda_{\text{max}} = 524$  ( $\epsilon$  2100 M<sup>−1</sup> cm<sup>−1</sup>) and 650 (1600 M<sup>−1</sup> cm<sup>−1</sup>) nm and is diamagnetic, which was attributed to antiferromagnetic coupling between the d<sup>9</sup> Cu(II) ion and the coordinated superoxide donor. In addition, IR spectroscopy revealed a  $\nu(^{16}\text{O}–^{16}\text{O})$  stretch at 964 cm<sup>−1</sup>, which shifted to 909 cm<sup>−1</sup> upon complete <sup>18</sup>O labeling. The results of mixed isotope labeling experiments (<sup>16</sup>O–<sup>18</sup>O) were interpreted to indicate that the superoxide is bound end-on. We note that the O–O stretching frequency observed for **78** is significantly lower in energy than that reported for the previously described side-on complex (1111 cm<sup>−1</sup>, as determined by resonance Raman spectroscopy). Allowing a THF solution of **78** to stand at ambient temperature eventually led to the formation of **77** and one equivalent of H<sub>2</sub>O<sub>2</sub>; a model reaction for the enzymatic step that regenerates Active GAO (Reduced GAO + O<sub>2</sub> → Active GAO + H<sub>2</sub>O<sub>2</sub>).

A final set of model complexes relevant to GAO involve the use of a highly redox active bis(phenol)phenylenediamine ligand (H<sub>4</sub>L<sup>8</sup>) [80]. As shown in Fig. 32, this ligand can exist in five different redox levels, related by successive one electron oxidation steps, resulting in species with either  $S = 0$  ([L<sup>8</sup>]<sup>4−</sup>, [L<sup>8</sup>]<sup>2−</sup> and [L<sup>8</sup>]<sup>0</sup>) or  $S = 1/2$  ([L<sup>8</sup>]<sup>3−</sup> and [L<sup>8</sup>]<sup>1−</sup>) ground states. In an extensive study performed by Wieghardt and coworkers it was discovered that all five of these redox states may serve as ligands to divalent Cu and Zn ions. Thus, ten complexes (**79**–**88**) have been generated (either chemically or electrochemically) and characterized by magnetic susceptibility and UV–vis and EPR spectroscopy (Table 9). Of particular interest to GAO model chemistry because of their ability to catalytically oxidize alcohols (Section 4) are complexes **82** and **87** derived from the reduced precursors **81** and **86**, respectively.

Reaction of H<sub>4</sub>L<sup>8</sup> with either [Cu(CH<sub>3</sub>CN)<sub>3</sub>](ClO<sub>4</sub>) or Zn(BF<sub>4</sub>)<sub>2</sub>·2H<sub>2</sub>O in MeOH under aerobic conditions yielded **81** or **86**. Note that these complexes are ligated by the 2-electron oxidized form of H<sub>4</sub>L<sup>8</sup>, [L<sup>8</sup>]<sup>2−</sup>. X-ray structural data revealed square planar geometries (cf. **81**, Fig. 33), with the coordination sphere made up of diiminoquinone and phenolate donors. Cyclic voltammetry performed on **81** or **86** revealed four reversible one electron processes over a range of 1.0 V to −1.0 vs. SCE. Similar potentials were observed for the Cu(II) and Zn(II) complexes, confirming the ligand based nature of these redox processes. Consistent with the electrochemical results, treatment of CH<sub>2</sub>Cl<sub>2</sub> solutions of **81** or **86** with one equivalent of ferrocenium hexafluorophosphate led to the formation of **82** and **87**, respectively (Fig. 34). This reaction involves oxidation of [L<sup>8</sup>]<sup>2−</sup> to [L<sup>8</sup>]<sup>1−</sup> ( $S = 1/2$  ground state) [81]. Temperature dependent magnetic susceptibility studies on solid **82** revealed antiferromagnetic coupling between the d<sup>9</sup> Cu(II) ion and the coordinated ligand-based organic radical with  $J = -48.5$  cm<sup>−1</sup> ( $H = -2JS_1S_2$ ). However, EPR studies performed on solutions of **82** suggested that the coupling is mainly intermolecular in nature, rather than intramolecular as believed to exist in the Cu(II)–phenoxyl radical complexes discussed earlier. As expected, **87** was found to be paramagnetic ( $\mu_{\text{eff}} = 1.8\mu_{\text{B}}$ ) due to the presence of one unpaired spin (diamagnetic Zn(II) ion and  $S = 1/2$  [L<sup>8</sup>]<sup>1−</sup>).

#### 4. Complexes that model the reactivity of GAO

As discussed above, a number of complexes containing phenoxyl radicals (or similar organic radicals) coordinated to a Cu(II) ion have been characterized. These complexes serve as both structural and spectroscopic models of the Active form of GAO. In addition, models for the Inactive and Reduced forms of the enzyme have

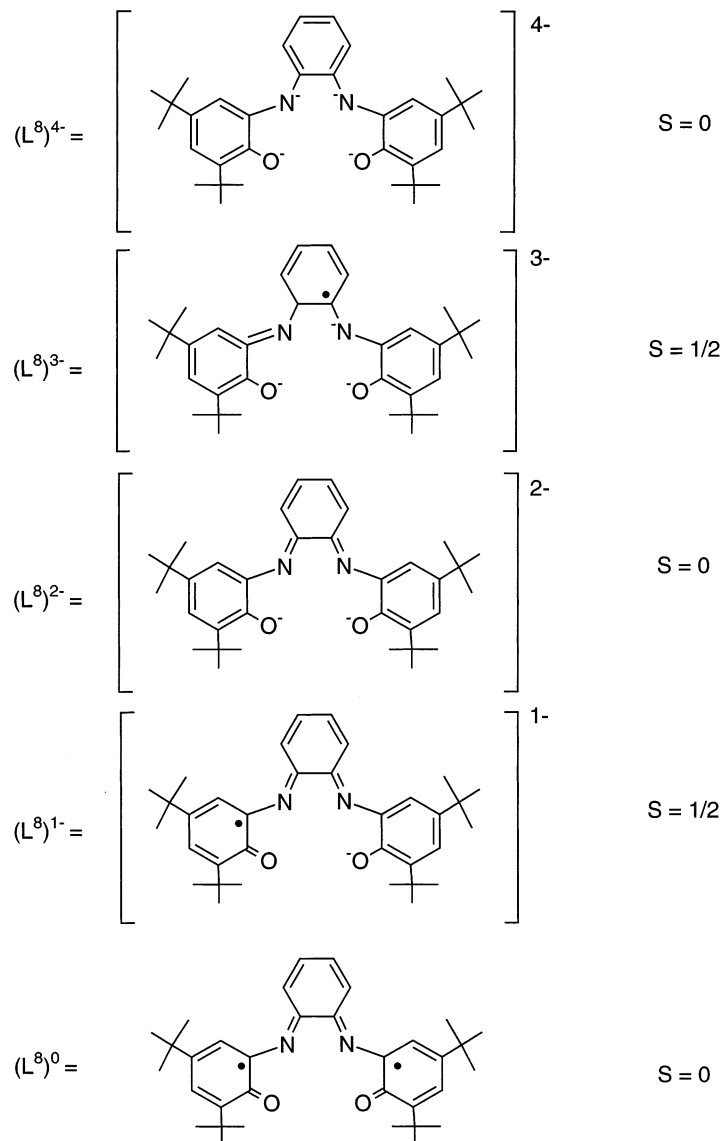


Fig. 32. Representations and electronic ground states of the five different redox levels of  $L^8$ .

Table 9

Summary of selected properties of Cu(II) and Zn(II) complexes of  $(L^8)^{n-}$  ( $n = 0-4$ ; all redox levels of the ligand are shown in Fig. 32)

No.	Formula	UV-vis <sup>a</sup>	EPR <sup>b</sup>
79	$[(H_2L^8)^2-Cu]^c$	453 (2500), 540 (sh), 700 (sh), 906 (2500)	$g_z = 2.278$ , $g_y = 2.067$ , $g_x = 2.059$ , $A_z = 183$ , $A_x = A_y = 11$
80	$[(L^8)^3-Cu]^{-d}$	330 (10800), 400 (sh), 607 (1900), 1073 (2500)	<sup>e</sup>
81	$[(L^8)^2-Cu]$	315 (9000), 356 (8500), 453 (2500), 483 (sh, 2200), 575 (1700), 747 (1800), 1256 (5600)	$g_z = 2.278$ , $g_y = 2.062$ , $g_x = 2.062$ , $A_z = 155$ , $A_x = A_y = 10$
82	$[(L^8)^1-Cu](PF_6)$	320 (5100), 478 (6400), 981 (1200)	$g_{eff} \approx 2.0$ , $g_{eff} \approx 4.0$
83	$[(L^8)^0Cu](ClO_4)_2$	311 (10000), 350 (sh), 455 (9100), 976 (1250)	$g_z = 2.224$ , $g_y = 2.076$ , $g_x = 2.044$ , $A_z = 156$ , $A_x = A_y = 32$
84	$[(H_2L^8)^2-Zn]$	700 ( $\approx 60$ )	—
85	$[(L^8)^3-Zn]^{-d}$	320 (9000), 401 (4000), 873 (6800)	$g = 2.0045$
86	$[(L^8)^2-Zn]$	405 (3000), 506 (4400), 798 (12200)	—
87	$[(L^8)^1-Zn](PF_6)$	385 (4200), 411 (3800), 578(2400), 810 (sh)	$g = 2.0045$
88	$[(L^8)^0Zn](ClO_4)_2$	326 (1200), 368 (1500), 392 (2900), 414 (2800), 500 (sh), 545 (8500), 700 (sh)	—

<sup>a</sup> All spectra in  $CH_2Cl_2$ .

<sup>b</sup> X-band EPR spectra recorded in  $CH_2Cl_2$ , with  $A$  values in units of  $10^{-4} \text{ cm}^{-1}$ .  $T = 10 \text{ K}$  for **79** and **81**,  $T < 70 \text{ K}$  for **80**,  $T = 50 \text{ K}$  for **82**,  $T = 4 \text{ K}$  for **83**,  $T = 298 \text{ K}$  for **85** and **87**.

<sup>c</sup> Generated in THF solution.

<sup>d</sup> Generated by controlled potential coulometry,  $0.10 \text{ M (Bu}_4\text{N)PF}_6$ .

<sup>e</sup> EPR silent at  $T < 70 \text{ K}$ , but broad spectrum at  $T > 80 \text{ K}$ .

been isolated. The knowledge gained from these structural/spectroscopic modeling studies provided the basis for attacking the problem of replicating enzymatic function. In this section we describe these efforts to mimic GAO activity, which have led to the discovery of the Cu–phenolate/phenoxyl radical (or related) model systems that perform alcohol oxidation, either stoichiometrically or catalytically, in some cases under quite mild conditions and with the concomitant conversion of  $O_2$  to  $H_2O_2$ .

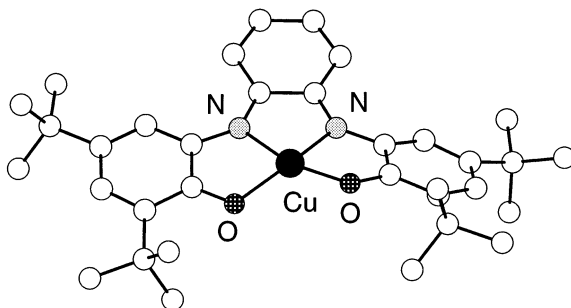


Fig. 33. X-ray crystal structure of the Cu(II) complex **81** of  $[L^8]^{2-}$  [80].

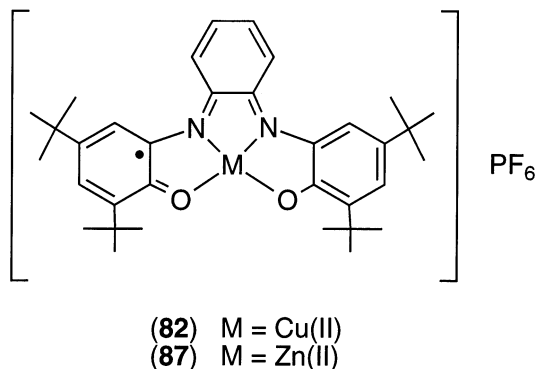


Fig. 34. Proposed structures of **82** and **87**, the products of oxidation of **81** and **86**, respectively.

A stoichiometric alcohol oxidation reaction that models the first phase of the proposed GAO catalytic cycle (Fig. 3) presaged the functional viability of synthetic Cu(II)–phenoxyl radical species. Electrochemical oxidation of **46** (Fig. 19) at 0.5 V vs. SCE led to the removal of an electron and bleaching of both UV and EPR spectral signals, implicating Cu(I) complex formation. Analysis of the product(s) revealed a 46% yield of benzaldehyde, suggesting that a Cu(II)–phenoxyl radical species was formed, but was not observable because it quickly reacted with the coordinated benzyl alcoholato substrate [48].

Alcohol oxidation by an observable Cu(II)–phenoxyl radical compound was reported later [37]. Treatment of a CH<sub>3</sub>CN solution of [**31**(NO<sub>3</sub>)]<sup>•+</sup> with excess benzyl alcohol yielded both benzaldehyde and Cu(I) product(s) (inferred from the absence of features in UV–vis and EPR spectra) (Fig. 35). Detailed kinetic analysis revealed an overall second order process (first order in both complex and substrate) and a competitive KIE of 6.8 (when PhCD<sub>2</sub>OH was used in place of PhCH<sub>2</sub>OH). These data are consistent with the mechanism shown in Fig. 35 wherein

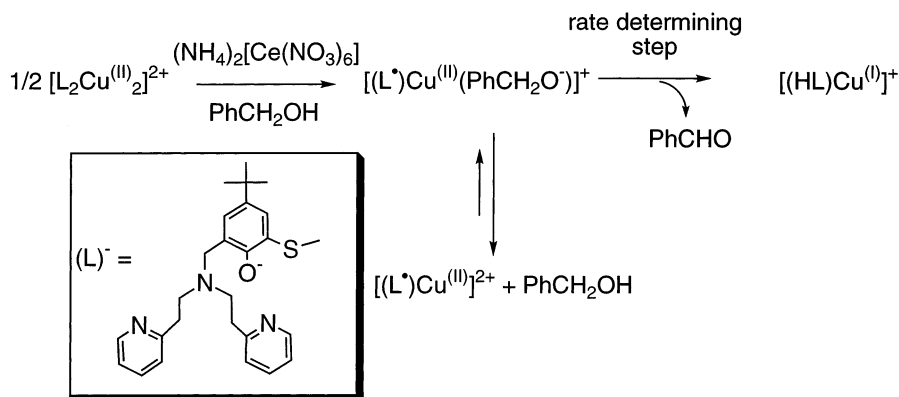


Fig. 35. Proposed mechanism for the stoichiometric oxidation of benzyl alcohol by [**31**<sup>•+</sup>] [37].

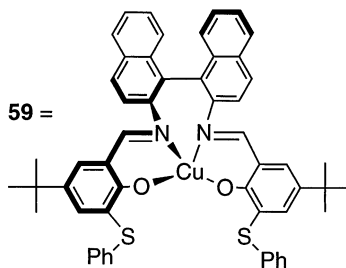


Fig. 36. Catalytic alcohol oxidation by **59** [64].

$[\mathbf{31}(\text{NO}_3)]^{\bullet+}$  functions as a 2-electron oxidant, shuttling between Cu(II)/Cu(I) and phenoxyl radical/phenolate, just as in GAO. Interestingly, alcohol oxidation was also observed using a Zn(II) analog, but the reaction rate was second-order with respect to the starting complex. This finding of a difference in mechanism between related Cu(II) and Zn(II) species confirms the importance of metal-based redox processes during the reaction.

In a preliminary demonstration of catalytic activity, albeit with sluggish rates and under harsh conditions, primary alcohols were oxidized by reaction of **57** (Fig. 21) with KOH and dioxygen in neat substrate (EtOH, *n*-PrOH, or hydroxyacetone) [64]. The corresponding aldehyde was formed, with as many as 12 turnovers observed (hydroxyacetone case) in 10 h. Use of other metal complexes of this same ligand (Ni(II), Co(II) or Zn(II)) led to no aldehyde production, emphasizing the necessity of Cu(II) for catalysis. No mechanistic information was provided. In related work which implicated the involvement of a Cu(II)–phenoxyl radical species in catalysis, treatment of the salen-containing Cu(II)–phenoxyl radical complex (**59**) $^{\bullet+}$  with excess  $\text{LiOCH}_2\text{Ph}$  and  $(\text{TPA})\text{SbCl}_6$  (20 equivalents each) in benzyl alcohol under anaerobic conditions yielded benzaldehyde (9.2 turnovers) (Fig. 36) [65a]. In another approach, bulk electrolysis of **66** (the Cu(II) complex of the reduced salen ligand shown in Fig. 20b) was performed at a potential sufficient to generate  $[\mathbf{66}]^{\bullet+}$  in the presence of primary alcohol (MeOH, EtOH, 1-PrOH or 1-BuOH), and KOH and the organic products were analyzed. For each primary alcohol surveyed the corresponding aldehyde was detected, with an identical turnover number of 32 in every case [67]. No ketone formation was observed when secondary alcohol substrates were used. The authors speculated that the efficiency of this complex as an alcohol oxidation complex may be limited due to substrate inaccessibility at a square planar active site.

Coupling of  $\text{O}_2$  reduction to  $\text{H}_2\text{O}_2$  with alcohol oxidation was achieved using complexes of some substituted salen ligands in neat allylic or benzylic alcohols with

only a catalytic amount of complex and base (Fig. 37) [65b]. Both aldehyde and  $\text{H}_2\text{O}_2$  were formed in a 1:1 ratio. Turnover numbers as high as 1300 after 20 h (complex **59** in neat benzyl alcohol) were observed. The catalytic cycle could be initiated by starting with either of three redox forms of the catalyst; Cu(II)–phenolate (**59**), Cu(II)–phenoxyl radical ( $\mathbf{59}^{\bullet+}$ ), or Cu(I)–phenolate (with the ligand of **59**). A similar number of turnovers was achieved in each case, but with different initial reaction rates. A possible catalytic mechanism is shown in Fig. 37. Much like in GAO, formation of a Cu(II)–(phenoxyl radical)(alcoholato) complex is believed to be followed by rate determining H-atom abstraction from the substrate. This notion is supported by observation of a competitive H/D KIE of 5.3 and a Hammett  $\rho$  value of  $-0.14$  (similar to those seen for H-atom abstractions by organic radicals) [82]. The Cu(I)-species formed as a result of electron transfer to

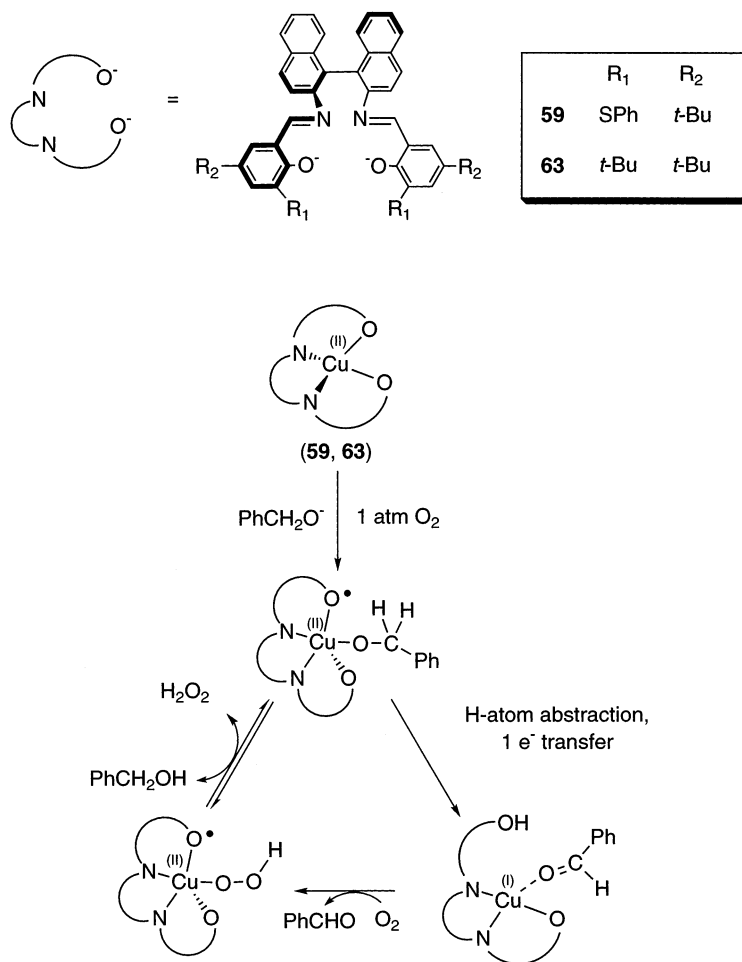


Fig. 37. Proposed mechanism for the catalytic oxidation of benzyl alcohol by **59** and **63** [64].

the metal center is proposed to react with  $O_2$  to form a Cu(II)–(phenoxyl radical)(hydroperoxide) species that has not been observed. Substrate binding would release  $H_2O_2$  and regenerate the active Cu(II)–(phenoxyl radical)(alcoholato) catalyst.

A more versatile catalytic system was developed using the dimeric complex **76** (Fig. 29). Addition of excess ethanol to an anaerobic THF solution of the complex led to the formation of one equivalent of acetaldehyde and a new copper-containing species, thought to be a tetra(phenolate)–Cu(II) dimer [75]. Exposure of this reaction mixture to  $O_2$  led to the regeneration of **76**, as well as the formation of one equivalent of  $H_2O_2$ . If the reaction was performed in the presence of  $O_2$ , catalytic ethanol oxidation was observed, with an overall yield of acetaldehyde as high as 63% (630 turnovers) in 12 h. Similar results were obtained with either benzyl alcohol or the secondary alcohol 2-butanol, yielding benzaldehyde and 2-butanone, respectively. A possible mechanism for these processes is shown in Fig. 38a. It is interesting to note that in the oxidation of ethanol and benzaldehyde, small amounts of 1,2-glycols,  $\alpha$ -hydroxyketones and  $\alpha$ -diketones were also detected. Furthermore, if 2-propanol or diphenylcarbinol were added as substrates, the 1,2-glycol products essentially were the sole products. A proposed mechanism for this alternative process is shown in Fig. 38b. Kinetics studies involving selective isotope labeling of substrate showed that the rate-determining step in both mechanisms is H-atom abstraction, much like in GAO. However, there are key differences in the overall mechanisms traversed by these systems and GAO. First, in both pathways (Fig. 38a and b) the active catalyst is believed to be dimeric in nature, as shown by a second-order dependence of the rate on the total Cu ion concentration and inhibition by added donors that presumably generate inactive monomeric species. Second, the proposed mechanisms only involve ligand-based redox processes; there is no shuttling between Cu(I) and Cu(II) states, in contrast to the proposed mechanism for GAO (Fig. 3). Still, unlike the functional models discussed above, **76** appears to be a more powerful oxidant capable of oxidizing EtOH and secondary alcohols.

In recent developments, complexes of ligands that can access multiple redox levels were found to be particularly efficient and reactive alcohol oxidation catalysts. One such system involved **77** (Fig. 31), which upon reaction with primary alcohols under anaerobic conditions yielded aldehyde and a Cu(I) product (proposed to be  $[(H_2L^{7-})Cu(NEt_3)]$ ). Catalytic aldehyde and  $H_2O_2$  production was observed when the reaction was performed in either THF solution or neat alcohol, under  $O_2$ , with yields as high as 55% and a rapid turnover frequency of  $0.5\ s^{-1}$  in neat benzyl alcohol. Unlike the previous example (**76**), no other alcohol oxidation products were observed and secondary alcohols were unaffected. Kinetic studies indicated that the active catalyst is mononuclear and that its activity is sensitive to the concentration of added  $NEt_3$ . A possible catalytic mechanism quite similar to that proposed for GAO is shown in Fig. 39. Substrate coordination to **77** is suggested to be followed by rate determining H-atom abstraction by the Cu(II)-imino-semiquinone species. Consistent with this proposal, a competitive H/D KIE of 8 was observed. Facile electron transfer leads to a Cu(I)–phenol(ate) product(s),

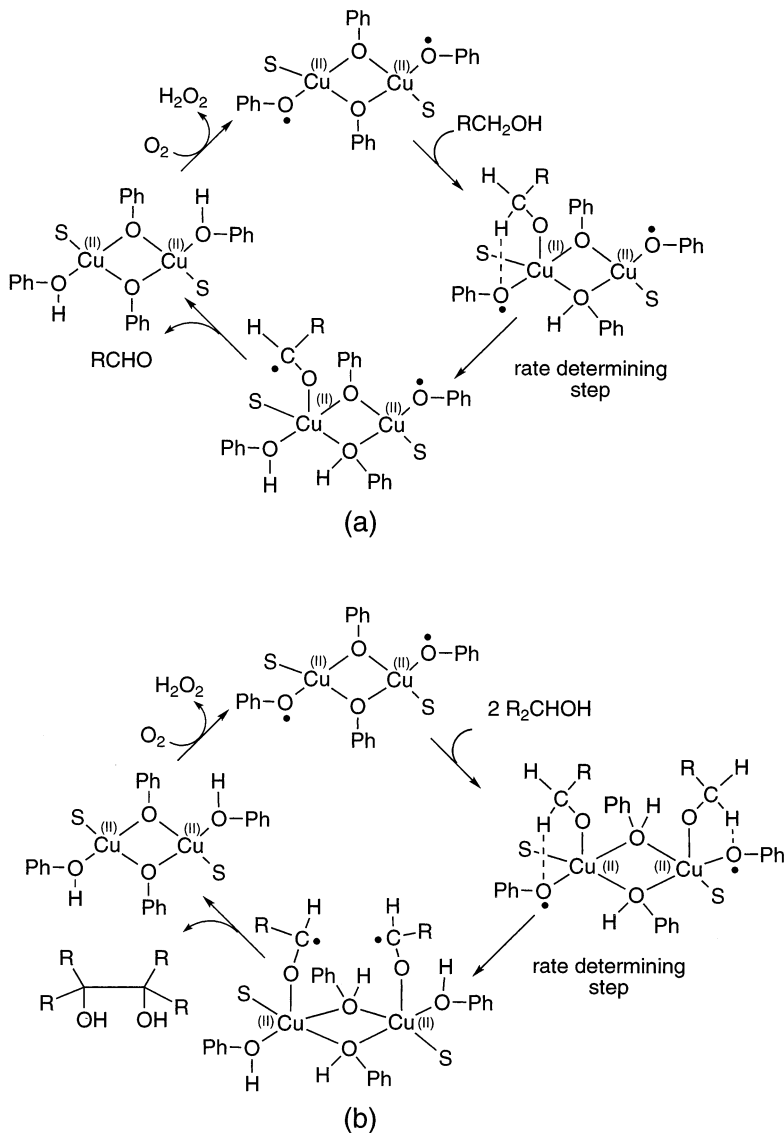


Fig. 38. Proposed mechanisms for the catalytic oxidation of primary and secondary alcohols by **76** to form either (a) aldehyde and ketone or (b) coupled 1,2-glycol products [75].

which may react with  $\text{O}_2$  to form **78**. The reaction cycle is completed upon release of  $\text{H}_2\text{O}_2$ , regenerating **77**.

An even more reactive system uses the divalent Cu and Zn complexes **82** and **87** (Fig. 34) to oxidize alcohols both stoichiometrically and catalytically. Anaerobic reaction of either complex with excess primary alcohol and two equivalents of  $\text{NEt}_3$  in  $\text{CH}_2\text{Cl}_2$  produced the corresponding aldehyde and **80** or **85** (as determined by

UV–vis spectroscopy). Affected substrates include EtOH and MeOH, but not the secondary alcohols 2-propanol or diphenylcarbinol. On the other hand, treatment of THF solutions of **82** or **87** with excess alcohol and  $\text{NEt}_3$  in the presence of air resulted in catalytic substrate oxidation, with production of aldehyde and  $\text{H}_2\text{O}_2$  in a 1:1 ratio. Approximately 5000 turnovers were observed with **82** and EtOH (turnover frequency =  $0.03 \text{ s}^{-1}$ , overall yield of ca. 50%) over a 40 h period, while **87** was found to be significantly less efficient (170 turnovers).

Extensive kinetic analyses of both single turnover and catalytic reactions are consistent with the mechanism shown in Fig. 40. In the first step, substrate is believed to reversibly bind to the mononuclear metal complex, thus forming a five-coordinate, square pyramidal complex. Consistent with this hypothesis, the catalytic rate was found to be affected by the concentration of  $\text{NEt}_3$ , which presumably acts as a competitive inhibitor for the available metal coordination site. Substrate binding is believed to be followed by rate determining H-atom abstraction. This proposal is supported the observation of significant H/D KIE's much higher than those discussed previously (as large as 54 for the single turnover experiment with **82** and MeOH). Such large KIE values are suggestive of a tunneling contribution to the reaction rate, as implicated in other metal-promoted

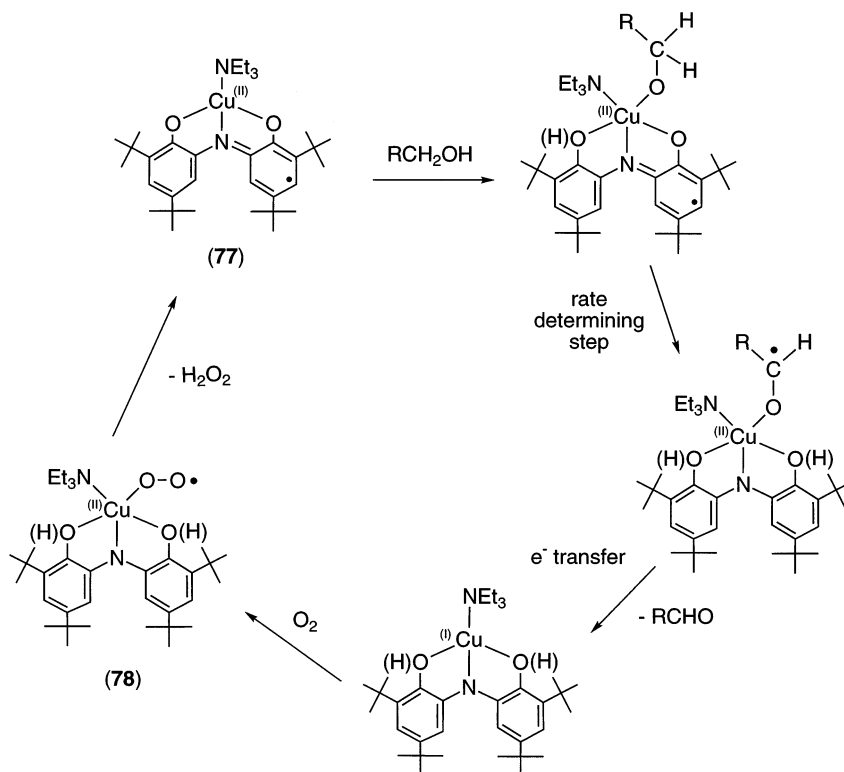


Fig. 39. Proposed mechanism for catalytic oxidation of primary alcohols by **77** with arbitrary proton placement for non-structurally characterized reaction intermediates [76].

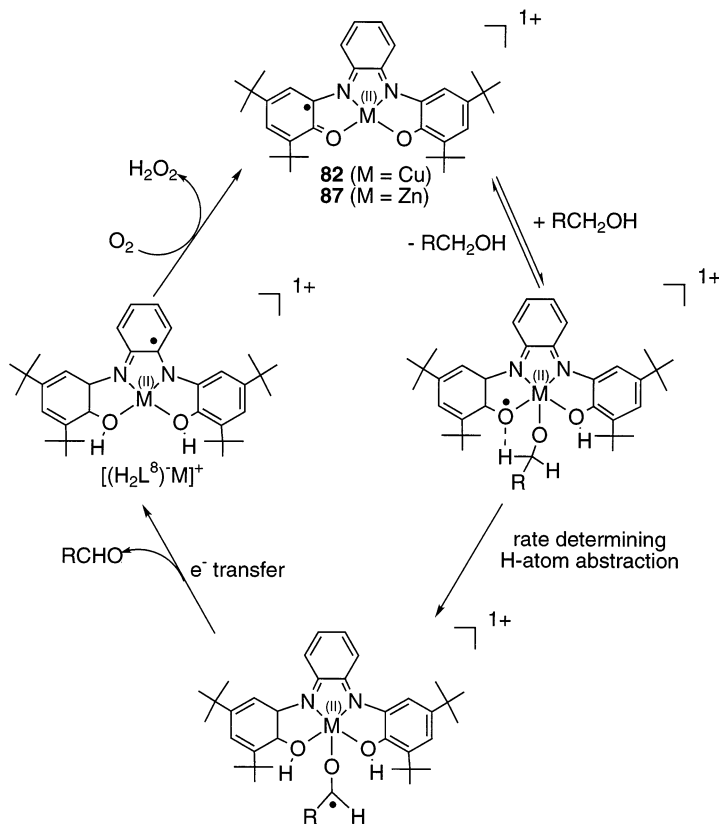


Fig. 40. Proposed mechanism for catalytic oxidation of primary alcohols by **82** and **87** [80].

oxidations [83]. Still, more extensive data and interpretation are required to corroborate this explanation. Of additional relevance was the discovery in a reaction of **82** with  $\beta$ -chloroethanol that succinic dialdehyde and Cl<sup>-</sup> were the primary products, not 2-chloroacetaldehyde (Fig. 41). This result implies that a ketyl radical derived from H-atom abstraction (but not hydride transfer) from substrate [24,25,80] quickly rearranges instead of undergoing rapid electron transfer to form 2-chloroacetaldehyde. In cases where non-halogenated primary alcohols were used, the coordinated ketyl radical (Fig. 40) rapidly transfers an electron to the metal complex, thus forming  $[(H_2L^8)^-M]^+$  and free aldehyde. This process is believed to involve ligand rather than metal reduction, but formation of a Cu(I) intermediate (in the case of **82**) cannot be ruled out. Reaction of  $[(H_2L^8)^-M]^+$  with O<sub>2</sub> is proposed to regenerate **82** or **87** and to release H<sub>2</sub>O<sub>2</sub>. The viability of this step was confirmed upon reaction of electrochemically generated  $[(H_2L^8)^-M]$  with O<sub>2</sub> in the presence of protons.

## 5. Conclusions

Through the work by a number of research groups on the synthesis and characterization of a range of Cu–phenolate and –phenoxyl radical complexes supported by a wide array of multidentate ligands, enormous progress has been made toward understanding the structural, spectroscopic, and functional attributes of the novel GAO active site. Close replication of many of the GAO active site properties has been achieved, including the structural and UV–vis, EPR, and resonance Raman features of the Inactive Cu(II)–tyrosinate form, the resonance Raman, magnetic, and aspects of the UV–vis features of the Active Cu(II)–tyrosyl radical form, and some of the structural features of the Reduced Cu(I)–phenol(ate) form. Together, in complementary fashion, the biochemical studies and the synthetic modeling work provide a comprehensive and detailed view of the key intermediates involved in GAO catalysis. Perhaps most importantly, this knowledge

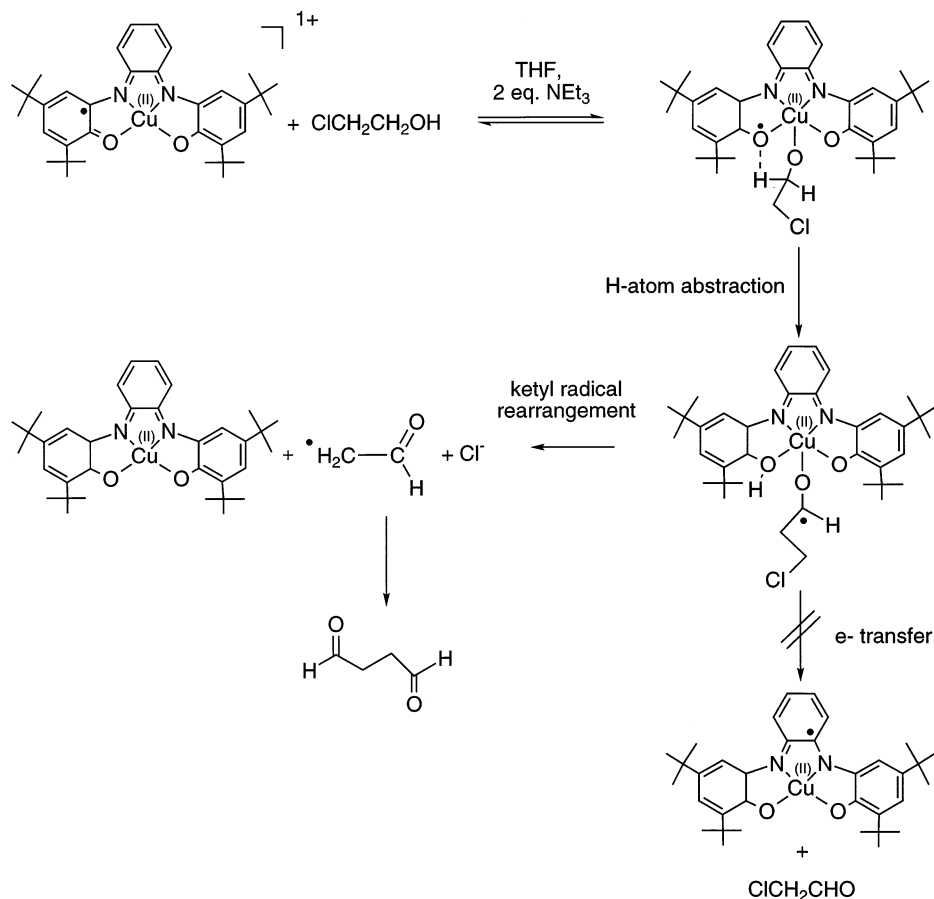


Fig. 41. Proposed mechanism for succinic dialdehyde production upon reaction of **82** with  $\beta$ -chloroethanol [76].

has led to the development of synthetic systems capable of performing stoichiometric and catalytic alcohol oxidation reactions by pathways closely akin to that followed by GAO. This type of ‘informed functional modeling’ whereby attributes of an enzymatic system are incorporated into the design of effective synthetic catalysts represents a remarkable feat in the bioinorganic chemistry field.

Our understanding is incomplete, however, and future research is needed to address key unresolved issues. The nature of the intense low-energy absorption feature in Active GAO has yet to be unraveled unequivocally. The relative importance of the stacking tryptophan and the cysteine modification of Y272 in controlling the redox potential of the coupled Cu–Y272 unit is not understood. The rates of the synthetic alcohol oxidation reactions are slow compared to the enzyme and the means by which the rate-controlling H-atom abstraction step may be accelerated in the biomimetic catalytic systems are not yet evident. Other mechanistic issues are unresolved, such as how Reduced GAO reacts with O<sub>2</sub> to yield Active GAO and H<sub>2</sub>O<sub>2</sub>; the details of this interesting step in both the enzyme and in synthetic models have yet to be determined. Finally, the mechanism of the Cu- and O<sub>2</sub>-dependent post-translational modification involving the coupling of Y272 and C228 is unknown. Future biochemical and synthetic modeling studies that address these and other issues are eagerly awaited.

## Acknowledgements

We thank the National Institutes of Health (GM47365) and the National Science Foundation (National Young Investigator Award) for financial support and Professor Karl Wieghardt for providing preprints describing work from his laboratory.

## References

- [1] J. Stubbe, W.A. van der Donk, *Chem. Rev.* 98 (1998) 705.
- [2] M. Fontecave, J.-L. Pierre, *Bull. Chim. Soc. Fr.* 133 (1996) 653.
- [3] J.W. Whittaker, in: H. Sigel, A. Sigel (Eds.), *Metalloenzymes Involving Amino Acid Residue and Related Radicals*, vol. 30, Marcel Dekker, New York, 1994.
- [4] (a) P.F. Knowles, N. Ito, in: *Perspectives on Bio-inorganic Chemistry*, vol. 2, Jai, London, 1993. (b) C.D. Borman, C.G. Sells, A. Sokolowski, M.B. Twitchett, C. Wright, A.G. Sykes, *Coord. Chem. Rev.* 190–192 (1999) 771.
- [5] (a) M.M. Whittaker, P.J. Kersten, N. Nakamura, J. Sanders-Loehr, E.S. Schweizer, J.W. Whittaker, *J. Biol. Chem.* 271 (1996) 681. (b) M.M. Whittaker, P.J. Kersten, D. Cullen, J.W. Whittaker, *J. Biol. Chem.* 274 (1999) 36226.
- [6] P.J. Kersten, *Proc. Natl. Acad. Sci.* 87 (1990) 2936.
- [7] H.-J. Krüger, *Angew. Chem. Int. Ed.* 38 (1999) 627.
- [8] J.P. Klinman, *Chem. Rev.* 96 (1996) 2541.
- [9] (a) J.W. Whittaker, in: J.P. Klinman (Ed.), *Methods in Enzymology, Redox-Active Amino Acids in Biology*, vol. 258, Academic, San Diego, 1995. (b) J.W. Whittaker, M.M. Whittaker, *Pure Appl. Chem.* 70 (1998) 903.

- [10] (a) N. Ito, S.E.V. Phillips, K.D.S. Yadav, P.F. Knowles, *J. Mol. Biol.* 238 (1994) 794. (b) N. Ito, S.E.V. Phillips, C. Stevens, Z.B. Ogel, M.J. McPherson, J.N. Keen, K.D.S. Yadav, P.F. Knowles, *Faraday Discuss.* 93 (1992) 75. (c) N. Ito, S.E.V. Phillips, C. Stevens, Z.B. Ogel, M.J. McPherson, J.N. Keen, K.D.S. Yadav, P.F. Knowles, *Nature* 350 (1991) 87. (d) N. Ito, P.F. Knowles, S.E.V. Phillips, in: J.P. Klinman (Ed.), *Methods in Enzymology, Redox-Active Amino Acids in Biology*, vol. 258, Academic, San Diego, 1995.
- [11] M.M. Whittaker, J.W. Whittaker, *J. Biol. Chem.* 263 (1988) 6074.
- [12] M.M. Whittaker, J.W. Whittaker, *Biophys. J.* 64 (1993) 762.
- [13] P.F. Knowles, R.D. Brown III, S.H. Koenig, S. Wang, R.A. Scott, M.A. McGuirl, D.E. Brown, D.M. Dooley, *Inorg. Chem.* 34 (1995) 3895.
- [14] K. Clark, J.E. Penner-Hahn, M.M. Whittaker, J.W. Whittaker, *J. Am. Chem. Soc.* 112 (1990) 6433.
- [15] (a) G.T. Babcock, M.K. El-Deeb, P.O. Sandusky, M.M. Whittaker, J.W. Whittaker, *J. Am. Chem. Soc.* 114 (1992) 3727. (b) F. Himo, G.T. Babcock, L.A. Eriksson, *Chem. Phys. Lett.* 313 (1999) 374.
- [16] M.L. McGlashen, D.D. Eads, T.G. Spiro, J.W. Whittaker, *J. Phys. Chem.* 99 (1995) 4918.
- [17] M.P. Reynolds, A.J. Brown, C.M. Wilmot, E. Vinecombe, C. Stevens, S.E.V. Phillips, P.F. Knowles, M.J. McPherson, *J. Biol. Inorg. Chem.* 2 (1997) 327.
- [18] M.M. Whittaker, J.W. Whittaker, *J. Biol. Chem.* 265 (1990) 9610.
- [19] A. Harriman, *J. Phys. Chem.* 91 (1987) 6102.
- [20] K.E. Silva, T.E. Elgren, L. Que, Jr., M.T. Stankovich, *Biochemistry* 34 (1995) 14093.
- [21] K. Clark, J.E. Penner-Hahn, M. Whittaker, J.W. Whittaker, *Biochemistry* 33 (1994) 12553.
- [22] M.M. Whittaker, D.P. Ballou, J.W. Whittaker, *Biochemistry* 37 (1998) 8426.
- [23] B.P. Branchaud, M.P. Montague-Smith, D.J. Kosman, F.R. McLaren, *J. Am. Chem. Soc.* 115 (1993) 798.
- [24] (a) R.M. Wachter, M.P. Montague-Smith, B.P. Branchaud, *J. Am. Chem. Soc.* 119 (1997) 7743. (b) B.E. Turner, B.P. Branchaud, *Bioorg. Med. Chem. Lett.* 9 (1999) 3341.
- [25] R.M. Wachter, B.P. Branchaud, *J. Am. Chem. Soc.* 118 (1996) 2782.
- [26] A. Maradufu, G.M. Cree, A.S. Perlin, *Can. J. Chem.* 49 (1971) 3429.
- [27] A related ligand with one pyridyl, one amine, one phenolate, and an amide (carbonyl O) donor also has been used to prepare a Cu(II)–phenolate complex: E.H. Alilou, E. Amadei, M. Giorgi, M. Pierrot, M. Réglér, *J. Chem. Soc. Dalton Trans.* (1993) 549.
- [28] K.D. Karlin, B.I. Cohen, J.C. Hayes, A. Farooq, J. Zubieta, *Inorg. Chem.* 26 (1987) 147.
- [29] U. Rajendran, R. Viswanathan, M. Palaniandavar, M. Lakshminarayanan, *J. Chem. Soc. Dalton Trans.* (1992) 3563.
- [30] R. Uma, R. Viswanathan, M. Palaniandavar, M. Lakshminarayanan, *J. Chem. Soc. Dalton Trans.* (1994) 1219.
- [31] H. Adams, N.A. Bailey, C.O.R.D. Barbarin, D.E. Fenton, Q.-Y. He, *J. Chem. Soc. Dalton Trans.* (1995) 2323.
- [32] H. Adams, N.A. Bailey, I.K. Campbell, D.E. Fenton, Q.-Y. He, *J. Chem. Soc. Dalton Trans.* (1996) 2233.
- [33] S. Ito, S. Nishino, H. Itoh, S. Ohba, Y. Nishida, *Polyhedron* 17 (1998) 1637.
- [34] K.D. Karlin, B.I. Cohen, *Inorg. Chim. Acta* 107 (1985) L17.
- [35] H. Adams, N.A. Bailey, D.E. Fenton, Q. He, M. Ohba, H. Okawa, *Inorg. Chim. Acta* 215 (1994) 1.
- [36] S. Itoh, S. Takayama, R. Arakawa, A. Furuta, M. Komatsu, A. Ishida, S. Takamuku, S. Fukuzumi, *Inorg. Chem.* 36 (1997) 1407.
- [37] S. Itoh, M. Taki, S. Takayama, S. Nagatomo, T. Kitagawa, N. Sakurada, R. Arakawa, S. Fukuzumi, *Angew. Chem. Int. Ed.* 38 (1999) 2774.
- [38] EPR data is reported for a number of Cu(II) complexes of L<sup>−</sup> (Fig. 4) with non-coordinating anions, although full spectroscopic characterization is lacking. See Ref. [30] for full details.
- [39] M.M. Whittaker, W.R. Duncan, J.W. Whittaker, *Inorg. Chem.* 35 (1996) 382.
- [40] D. Zurita, C. Scheer, J.-L. Pierre, E. Saint-Aman, *J. Chem. Soc. Dalton Trans.* (1996) 4331.
- [41] D. Zurita, I. Gautier-Luneau, S. Ménage, J.-L. Pierre, E. Saint-Aman, *J. Biol. Inorg. Chem.* 2 (1997) 46.

- [42] Throughout this article, electrochemical potentials are cited relative to the standard calomel electrode (SCE). In cases where potentials are reported versus other standards, corrections were applied as described in the following papers in order to facilitate comparisons between systems. We note that differences in solvent, electrolyte identity and concentrations, and other factors complicate such comparisons. (a) C.K. Mann, K.K. Barnes, *Electrochemical Reactions in Non-aqueous Systems*, Marcel Dekker, New York, 1990. (b) N.G. Connolly, W.E. Geiger, *Chem. Rev.* 96 (1996) 877.
- [43] Similar behavior was reported for complex **35**: D. Zurita, S. Ménage, J.-L. Pierre, E. Saint-Aman, *New J. Chem.* 21 (1997) 1001.
- [44] Monomeric Cu complexes could also be independently generated when the syntheses of **33** and **34** were performed in the absence of base (Fig. 10).
- [45] P. Chaudhuri, K. Wieghardt, *Prog. Inorg. Chem.* 35 (1988) 329.
- [46] J. Hockertz, S. Steenken, K. Wieghardt, P. Hildebrandt, *J. Am. Chem. Soc.* 115 (1993) 11222.
- [47] U. Auerbach, U. Eckert, K. Wieghardt, B. Nuber, J. Weiss, *Inorg. Chem.* 29 (1990) 938.
- [48] J.A. Halfen, V.G. Young, Jr., W.B. Tolman, *Angew. Chem. Int. Ed.* 35 (1996) 1687.
- [49] A. Sokolowski, H. Leutbecher, T. Weyhermüller, R. Schnepf, E. Bothe, E. Bill, P. Hildebrandt, K. Wieghardt, *J. Biol. Inorg. Chem.* 2 (1997) 444.
- [50] J.A. Halfen, B.A. Jazdzewski, S. Mahapatra, L.M. Berreau, E.C. Wilkinson, L. Que, Jr., W.B. Tolman, *J. Am. Chem. Soc.* 35 (1997) 8217.
- [51] J. Müller, T. Weyhermüller, E. Bill, P. Hildebrandt, L. Ould-Moussa, T. Glaser, K. Wieghardt, *Angew. Chem. Int. Ed.* 37 (1998) 616.
- [52] E. Bill, J. Müller, T. Weyhermüller, K. Wieghardt, *Inorg. Chem.* 38 (1999) 5795.
- [53] A. Sokolowski, J. Müller, T. Weyhermüller, R. Schnepf, P. Hildebrandt, K. Hildenbrand, E. Bothe, K. Wieghardt, *J. Am. Chem. Soc.* 119 (1997) 8889.
- [54] R.J. Motekaitis, Y. Sun, A.E. Martell, *Inorg. Chim. Acta* 198–200 (1992) 421.
- [55] E.T. Clarke, A.E. Martell, *Inorg. Chim. Acta* 186 (1991) 103.
- [56] (a) L. Que, Jr., in: T.G. Spiro (Ed.), *Biological Applications of Raman Spectroscopy*, vol. 3, Wiley, New York, 1988. (b) L. Que, Jr., *Coord. Chem. Rev.* 50 (1983) 73.
- [57] A. Mukherjee, M.L. McGlashen, T.G. Spiro, *J. Phys. Chem.* 99 (1995) 4912.
- [58] (a) A. Sokolowski, E. Bothe, E. Bill, T. Weyhermüller, K. Wieghardt, *Chem. Commun.* (1996) 1671. (b) B. Adam, E. Bill, E. Bothe, B. Goerdts, G. Haselhorst, K. Hildenbrand, A. Sokolowski, S. Steenken, T. Weyhermüller, K. Wieghardt, *Chem. Eur. J.* 3 (1997) 308. (c) A. Sokolowski, B. Adam, T. Weyhermüller, A. Kikuchi, K. Hildenbrand, R. Schnepf, P. Hildebrandt, E. Bill, K. Wieghardt, *Inorg. Chem.* 36 (1997) 3702. (d) R. Schnepf, A. Sokolowski, J. Müller, V. Bachler, K. Wieghardt, P. Hildebrandt, *J. Am. Chem. Soc.* 120 (1998) 2352. (e) M.D. Snodin, L. Ould-Moussa, U. Wallman, S. Lecomte, V. Bachler, E. Bill, H. Hummel, T. Weyhermüller, P. Hildebrandt, K. Wieghardt, *Chem. Eur. J.* 5 (1999) 2554.
- [59] E.R. Altwick, *Chem. Rev.* 67 (1967) 475.
- [60] (a) D.P. Goldberg, S.J. Lippard, in: H.H. Thorp, V.L. Pecoraro (Eds.), *Advances in Chemistry*, vol. 246, American Chemical Society, Washington, DC, 1995. (b) D.P. Goldberg, S.P. Watton, A. Masschelein, L. Wimmer, S.J. Lippard, *J. Am. Chem. Soc.* 115 (1993) 5346. (c) D.P. Goldberg, D. Koulougliotis, G.W. Brudvig, S.J. Lippard, *J. Am. Chem. Soc.* 117 (1995) 3134.
- [61] (a) G.N.R. Tripathi, R.H. Schuler, *J. Phys. Chem.* 92 (1988) 5129. (b) Y. Qin, R.A. Wheeler, *J. Am. Chem. Soc.* 117 (1995) 6083 and references cited therein.
- [62] (a) D. Hall, T.N. Waters, *J. Chem. Soc.* (1960) 2644. (b) E.N. Baker, D. Hall, T.N. Waters, *J. Chem. Soc. (A)* (1970) 406. (c) M.B. Ferrari, G.G. Fava, C. Pelizzi, *Acta Crystallogr. Sect. B* 32 (1976) 901. (d) P. Cassoux, A. Gleizes, *Inorg. Chem.* 19 (1980) 665.
- [63] (a) T.P. Cheeseman, D. Hall, T.N. Waters, *J. Chem. Soc. (A)* (1966) 1396. (b) N. Galesic, R. Trojko, Z. Cimerman, Z. Stefanac, *Acta Crystallogr. C* 40 (1984) 232. (c) K. Bernardo, S. Leppard, A. Robert, G. Commenges, F. Dahan, B. Meunier, *Inorg. Chem.* 35 (1996) 387.
- [64] N. Kitajima, K. Whang, Y. Moro-oka, A. Uchida, Y. Sasada, *J. Chem. Soc. Chem. Commun.* (1986) 1504.
- [65] (a) Y. Wang, T.D.P. Stack, *J. Am. Chem. Soc.* 118 (1996) 13097. (b) Y. Wang, J.L. DuBois, B. Hedman, K.O. Hodgson, T.D.P. Stack, *Science* 279 (1998) 537.

- [66]  $\text{TPA}^+ = \text{tris(4-bromophenyl)aminium}$ .
- [67] E. Saint-Aman, S. Ménage, J.-L. Pierre, E. Defrancq, G. Gellon, *New J. Chem.* (1998) 393.
- [68] (a) S. Trofimenko, *Chem. Rev.* 93 (1993) 943. (b) N. Kitajima, W.B. Tolman, *Prog. Inorg. Chem.* 43 (1995) 419.
- [69] M. Ruf, C.G. Pierpont, *Angew. Chem. Int. Ed.* 37 (1998) 1736.
- [70] (a) M.A. Halcrow, L.M.L. Chia, X. Liu, E.J.L. McInnes, L.J. Yellowlees, F.E. Mabbs, J.E. Davies, *Chem. Commun.* (1998) 2465. (b) M.A. Halcrow, L.M.L. Chia, X. Liu, E.J.L. McInnes, L.J. Yellowlees, F.E. Mabbs, I.J. Scowen, M. McPartlin, J.E. Davies, *J. Chem. Soc. Dalton Trans.* (1999) 1753.
- [71] M.M. Whittaker, Y.-Y. Chuang, J.W. Whittaker, *J. Am. Chem. Soc.* 115 (1993) 10029.
- [72] A search of the Cambridge Crystallographic Database (vol. 5.17) revealed no examples of monomeric Cu(I) complexes with a coordinated phenol ligand, and only three examples of monomeric Cu(I)–phenolate complexes.
- [73] T.N. Sorrell, A.S. Borovik, C.C. Shen, *Inorg. Chem.* 25 (1986) 589–590.
- [74] B.A. Jazdzewski, V.G. Young, Jr., W.B. Tolman, *Chem. Commun.* (1998) 2521.
- [75] P. Chaudhuri, M. Hess, U. Flörke, K. Wieghardt, *Angew. Chem. Int. Ed.* 37 (1998) 2217.
- [76] P. Chaudhuri, M. Hess, T. Weyhermüller, K. Wieghardt, *Angew. Chem. Int. Ed.* 38 (1999) 1095.
- [77] (a) A.Y. Girgis, A.L. Balch, *Inorg. Chem.* 14 (1975) 2724. (b) C.L. Simpson, S.R. Boone, C.G. Pierpont, *Inorg. Chem.* 28 (1989) 4379. (c) S.K. Larsen, C.G. Pierpont, *J. Am. Chem. Soc.* 110 (1988) 1827. (d) S. Bruni, A. Caneschi, F. Cariati, C. Delfs, A. Dei, D. Gatteschi, *J. Am. Chem. Soc.* 116 (1994) 1388. (e) G. Speier, J. Csihony, A.M. Whalen, C.G. Pierpont, *Inorg. Chem.* 35 (1996) 3519.
- [78] Note that  $\text{H}_2\text{L}^{7-}$  refers to the doubly protonated form of  $[\text{L}^7]^{3-}$  (Fig. 30).
- [79] K. Fujisawa, M. Tanaka, Y. Moro-oka, N. Kitajima, *J. Am. Chem. Soc.* 116 (1994) 12079.
- [80] P. Chaudhuri, M. Hess, J. Müller, K. Hildenbrand, E. Bill, T. Weyhermüller, K. Wieghardt, *J. Am. Chem. Soc.* 121 (1999) 9599.
- [81] Similar complexes also could be generated upon reaction of  $\text{H}_4\text{L}^8$  with CuCl or  $\text{Zn}(\text{ClO}_4)\cdot 6\text{H}_2\text{O}$  in THF with subsequent exposure to air.
- [82] G.A. Russell, in: J.K. Kochi (Ed.), *Free Radicals*, vol. I, Wiley, New York, 1973.
- [83] For example, see: (a) L. Roecker, T.J. Meyer, *J. Am. Chem. Soc.* 109 (1987) 746. (b) O.M. Reinaud, K.H. Theopold, *J. Am. Chem. Soc.* 116 (1994) 6979. (c) S. Mahapatra, J.A. Halfen, W.B. Tolman, *J. Am. Chem. Soc.* 118 (1996) 11575 and references cited therein. (d) E.L. Lebeau, T.J. Meyer, *Inorg. Chem.* 38 (1999) 2174.